CENTRAL RESEARCH LIBRARY
DOCUMENT COLLECTION

1

OAK RIDGE NATIONAL LABORATORY
operated by
UNION CARBIDE CORPORATION
NUCLEAR DIVISION
for the
U.S. ATOMIC ENERGY COMMISSION

ORNL-TM-2622

MARTIN MARIETTA ENERGY SYSTEMS LIBRARIES
3 4456 0135106 9

OPTICAL CONSTANTS OF CESIUM FOR PHOTONS OF ENERGY 5 TO 9.6 eV

(Thesis)

U. S. Whang, T. A. Callcott, and E. T. Arakawa

OAK RIDGE NATIONAL LABORATORY
CENTRAL RESEARCH LIBRARY
DOCUMENT COLLECTION
LIBRARY LOAN COPY
DO NOT TRANSFER TO ANOTHER PERSON
If you wish someone else to see this document, send in name with document and the library will arrange a loan.
UCN-7969
(3 3-67)

Submitted by U. S. Whang as a dissertation to the Graduate School of The University of Tennessee in partial fulfillment of the requirements for the degree of Master of Science.

LEGAL NOTICE

This report was prepared as an account of Government sponsored work. Neither the United States, nor the Commission, nor any person acting on behalf of the Commission:

A. Makes any warranty or representation, expressed or implied, with respect to the accuracy, completeness, or usefulness of the information contained in this report, or that the use of any information, apparatus, method, or process disclosed in this report may not infringe privately owned rights; or

B. Assumes any liabilities with respect to the use of, or for damages resulting from the use of any information, apparatus, method, or process disclosed in this report.

As used in the above, "person acting on behalf of the Commission" includes any employee or contractor of the Commission, or employee of such contractor, to the extent that such employee or contractor of the Commission, or employee of such contractor prepares, disseminates, or provides access to, any information pursuant to his employment or contract with the Commission, or his employment with such contractor.

ORNL-TM-2622

Contract No. W-7405-eng-26

HEALTH PHYSICS DIVISION

OPTICAL CONSTANTS OF CESIUM FOR PHOTONS OF ENERGY 5 TO 9.6 eV

U. S. Whang, T. A. Callcott, and E. T. Arakawa

Submitted by U. S. Whang as a dissertation to the
Graduate School of The University of Tennessee
in partial fulfillment of the requirements
for the degree of
Master of Science

MARCH 1970

OAK RIDGE NATIONAL LABORATORY
Oak Ridge, Tennessee
operated by
UNION CARBIDE CORPORATION
for the
U. S. ATOMIC ENERGY COMMISSION

MARTIN MARIETTA ENERGY SYSTEMS LIBRARIES

3 4456 0135106 9

ACKNOWLEDGEMENTS

The author wishes to thank Dr. T. A. Callcott for his enthusiastic guidance and friendship throughout the course of this work. He also takes great pleasure in expressing his sincere appreciation to Drs. E. T. Arakawa, H. C. Schweinler, R. H. Ritchie, and R. N. Hamm for their constant instructions and helpful discussions, and to Dr. R. D. Birkhoff for his special concern and encouragement for this work.

A consultant subcontract with Union Carbide Corporation, Nuclear Division, ORNL, and a graduate research assistantship supported by NSF should be acknowledged. Gratitude is expressed for use of the research facilities in the Health Physics Division of the Oak Ridge National Laboratory, where the research was sponsored by the U.S. Atomic Energy Commission under contract with Union Carbide Corporation.

The author wishes to present this accomplishment to his parents for their enduring love and understanding.

ABSTRACT

The optical constants of cesium films evaporated onto CaF_2 substrates at 10^{-6} Torr have been determined in the spectral region from 1294 Å (9.59 eV) to 2377 Å (5.22 eV) from the critical angle marking the onset of total reflection. The refractive index n is determined from the critical angle of the reflectance curves of each wavelength. The absorption coefficient k is estimated from the slope of the curve at the critical angle. The real part of the complex dielectric constant ϵ_1 is consistent with a nearly free-electron model for photon energies less than 7.7 eV (1613 Å). For photon energies greater than 7.7 eV, ϵ_1 is greater than the nearly free-electron model would predict. This effect is attributed to the existence of transitions from inner shells at energies $\gtrsim 11.4$ eV. The measured optical parameters are $m_{opt}/m = 1.25$, $\hbar\omega_p = 2.85$ eV, and $4\pi n_o \alpha_1 = .20$. In ϵ_2 we find a broad peak centered at about 4.5 eV. This optical absorption may be explained by the existence of plasmon-assisted transitions.

TABLE OF CONTENTS

CHAPTER	PAGE
I. INTRODUCTION	1
II. SURVEY OF PREVIOUS RESULTS	4
III. THEORY	7
Optical Constants	7
Optical Properties	10
Classical free electron theory	10
Quantum mechanical theory	18
Reflectance and Transmittance of Light at Non-Normal Incidence	26
IV. EXPERIMENTAL APPARATUS	29
V. EXPERIMENTAL PROCEDURE	37
Alignment of the Optical System	37
Preparation of Cesium Film	38
Reflectance Measurements	39
Determination of Background	40
Determination of the Polarization of the Incident Light	41
VI. DETERMINATION OF OPTICAL CONSTANTS	44
VII. DISCUSSION OF RESULTS	63
BIBLIOGRAPHY	75
VITA	80

LIST OF FIGURES

FIGURE		PAGE
1.	Behavior of ϵ_1 and ϵ_2 as a Function of ω for Free Electrons . .	13
2.	Dependence of $\epsilon_1 - 1$ and $\omega\epsilon_2$ on Frequency for a Single Resonant Absorption	16
3.	Energy Bands of Cesium Along a (1, 1, 0) Axis	20
4.	Schematic Diagram of Apparatus	30
5.	Schematic Diagram of Reflectance Chamber and Angle Doubler	33
6.	Diagram of Semicylinder	35
7.	Polarization of 1500 Å Blaze Grating as a Function of Wavelength	43
8.	Calculated Reflectance versus Angle of Incidence for $n_{rel} = .7$, $\theta_c = 44° 26'$, and Different Values of k_{rel}	46
9.	Index of Refraction of Calcium Fluoride as a Function of Wavelength	48
10.	Dependence of the Slope of the Reflectance at θ_m on n_{rel} and P	49
11.	The Change in Reflectance of the Cesium Film (Thick Film) Due to Formation of an Oxide Layer for $\lambda = 1295$ Å	51
12.	The Change in Reflectance of the Cesium Film (Thin Film) Due to Formation of an Oxide Layer for $\lambda = 1536$ Å	52

FIGURE PAGE

13. The Change in Reflectance of the Cesium Film (Thick Film) Due to Formation of an Oxide Layer for $\lambda = 1477 Å$ 53

14. The Change in Reflectance of the Cesium Film (Thick Film) Due to Formation of an Oxide Layer for $\lambda = 1761 Å$ 54

15. Fitting of Experimental Reflectance at 1817 Å (O) and 2260 Å (Δ) to Theoretical Curves 59

16. Experimentally Determined n and k for Cesium 61

17. Real Part of the Complex Dielectric Constant versus Square of Photon Energy 64

18. Optical Conductivity versus Photon Energy ($\hbar\omega$) 69

CHAPTER I

INTRODUCTION

The alkalies are the simplest of the metals in that their properties most nearly match those predicted using a simple nearly-free-electron model of metals. In addition, the relative ease of first principle calculations involving these materials generates theoretical interest in their optical and other properties.

As atoms, the alkalies have a single s electron lying outside closed shell ion cores. When condensed into a solid, the closed shells form small ion cores with a positive charge that have little effect on bonding of the solid. The outer electrons overlap strongly and account for most of the solid properties.

Most of the optical properties of the alkalies can be accounted for on the basis of an independent particle model. In this model the energy levels of the electrons can be found by solving a Schrödinger equation for one electron in the potential field of the ions and the remaining electrons. The resulting charge density is nearly constant over about 90% of the volume of the metals with the result that electrons have energy states as a function of crystal momentum only slightly different from those of free electrons.

Within the independent particle framework the simplest model is that of Drude (1900) and Lorentz (1903) which was developed before the advent

of the quantum theory. They treated free electrons as particles driven by a sinusoidally varying electric field vector and damped by a velocity-dependent damping function. The damping constant was calculated for specific solids by relating it to d. c. conductivity. The results of this theory are given in Chapter III. Later quantum mechanical calculations gave added substance to the theory by confirming its general results and making it possible to calculate the damping constant [Cohen (1958), Kronig (1934), Fröhlich (1933), Fujioka (1932), Wilson (1935, 1953), Mott and Jones (1936)]. This theory accounts for the most striking features of the optical properties of the alkalies; namely, that they are highly reflecting in the visible and infrared and transparent in the ultraviolet. The critical frequency separating the two regions is called the plasma frequency. It has a value of 5.42 eV (2100 Å) for sodium and decreases with increasing atomic number to 2.80 eV (4400 Å) for cesium.

In the transparent region, with which we are particularly concerned in this study, the Drude theory is inadequate in two major respects. It fails to account for a dielectric constant and index of refraction greater than one, and it fails to account for the observed optical absorption. Both of these effects are in large measure related to the existence of direct transition (without lattice interaction) between one electron states in the metals. These effects can be readily accounted for with the independent particle quantum mechanical model described in Chapter III. The study of these direct transition effects is a major goal of this investigation.

Polarization of core electrons contributes to the real part of the complex dielectric constant. This is the effect due to the displacement of electrons in an atom relative to the nucleus, that is, due to the deformation of the electron shell relative to the nucleus when an electric field is applied. This effect is also naturally accounted for in the quantum mechanical treatment of Chapter III.

However, independent-particle theory is probably inadequate to account for all observed absorption. It seems probable, on the basis of our data, that many-body effects [Hopfield (1965), Pines (1964), Seitz (1940)] are involved as well. Various absorption mechanisms have been suggested by Hopfield (1965) and Cohen (1964).

A major reason for studying optical properties in cesium is that both interband absorption and many-body effects seem to be stronger in this metal than in the other alkalies. The studies are of particular interest because a plasmon-assisted optical absorption mechanism has not yet been experimentally demonstrated in cesium.

In Chapter II a description is given of previous theoretical and experimental results on the optical properties of cesium.

CHAPTER II

SURVEY OF PREVIOUS RESULTS

The first measurements of the optical constants of cesium were made by Nathanson (1925). He found that the index of refraction varied from .362 for photon wavelength 4550 Å to .350 for 6800 Å, and that the coefficient of absorption increased from 2.37 for 4550 Å to 4.34 for 6800 Å. He also calculated the reflectance and computed the number of free electrons per atom according to Drude's (1904) theory to find a larger value of the optical conductivity than that of electrical conductivity.

Wood (1933a) showed that the transmission band began at about 4400 Å for cesium from the measurement of the reflectance of cesium in its transparent region between 3100 Å and 4400 Å, and suggested that the dispersion of cesium could be determined from both its Brewster's angle and its critical angle in this region. Wood and Lukens (1938) showed that cesium and other alkali metals were transparent to radiation of wavelength down to 500 Å.

Zener (1933) explained the transparency of the alkali metals in the ultraviolet and their high reflectance in the visible portion of the spectrum as a consequence of the Drude-Lorentz-Kronig [Kronig (1929, 1931)] free-electron model of metallic structure. The critical wavelength at which transparency starts occurs when the dielectric constant of the metal

is zero. For cesium it was calculated from the free-electron theory to be 3600 Å. Kronig (1934) extended Zener's free-electron treatment of the problem to include damping of the conduction electrons. He thus showed that reflectance of slightly less than 100% was explained for wavelengths greater than the critical wavelength, and also pointed out that the electrons were not completely free as assumed.

Measurements of the optical constants of cesium were made by Ives and Briggs (1937b) at wavelengths ranging from the ultraviolet (2536 Å) to the visible region (5780 Å) of the spectrum. They attempted to fit their data by neglecting the atomic polarizability and interband absorption and found very poor agreement for cesium, while they (1937a) found good agreement for sodium. Cohen (1958) analyzed the data of Ives and Briggs in terms of a quantum mechanical theory of the optical properties of a metal by simplifying the general theory of the optical constants of metals. The theory took into account the periodic structure of the metallic crystal and the core electrons, in addition to the free conduction electrons, and good agreement with the experimental results was obtained. From the experimental data, Cohen deduced values for the ion-core polarization, plasma wavelength, and optical effective mass of the conduction electrons of the metal.

Recently Mayer and Hietel (1966) measured the optical properties of cesium from the ultraviolet (2968 Å) to the infrared (25,000 Å) under

ultrahigh-vacuum conditions. They found an absorption at 1.2 eV in cesium which is attributed to interband transitions, and they reported anomalous absorptions in the other alkali metals. In addition, they showed that the anomalous absorptions were temperature dependent. Several theoretical attempts have been made to explain the anomalous absorptions of these alkali metals [Cohen and Phillips (1964), Cohen (1964, 1966), Ferrell (1966), Overhauser (1964), Appelbaum (1966), Nettel (1966)]. Cohen (1966) pointed out that the rise of absorption in cesium by Mayer and Hietel (1966) in the ultraviolet region could be due to the plasma resonance predicted by Hopfield (1965).

Payan and Roux (1968) measured the absorption for thin layers of cesium. They found quite good agreement between their results for thin layers in the region above 3 eV of photon energy and the absorption reported by Mayer and Hietel for the bulk metal. They found a broad peak at about 2 eV but did not find a sharp rise in the absorption at about 1.2 eV as reported by Mayer and Hietel.

CHAPTER III

THEORY

I. OPTICAL CONSTANTS

The propagation of light in an absorbing medium is described by the complex refractive index

$$\tilde{n} = n + ik \, . \tag{1}$$

The real part of the refractive index, n, is defined as the ratio of the velocity of light in vacuum, c, to the phase velocity in the medium, v, of a plane electromagnetic wave having constant amplitude along a wave front,

$$n = c/v \, . \tag{2}$$

The imaginary part of the complex refractive index, k, called the extinction or absorption coefficient, is defined such that the amplitude of the radiation is spatially damped by a factor $\exp(-\frac{k\omega}{c} z)$ or $\exp(-\frac{2\pi k}{\lambda} z)$ when the wave of vacuum wavelength λ traverses a distance z in the direction of propagation.

Considering the x-component of the electric intensity of radiation of energy $\hbar\omega$ moving in the positive z-direction through the material characterized by $\tilde{n}$, the propagating wave may be described by the equation

$$E_x(z, t) = E_x^o \exp\left[i\left(\frac{2\pi n}{\lambda} z - \omega t\right)\right] \exp\left[-\frac{2\pi k}{\lambda} z\right] . \tag{3}$$

Thus the equation for radiation passing through a transparent material is modified by an absorption term.

In classical macroscopic theory for an uncharged polarizable conducting medium Maxwell's equations are

$$\nabla \times \vec{E} = -\frac{1}{c}\frac{\partial \vec{H}}{\partial t}, \qquad \nabla \cdot \vec{E} = 0$$

$$\nabla \times \vec{H} = \frac{\epsilon}{c}\frac{\partial \vec{E}}{\partial t} + \frac{4\pi\sigma}{c}\vec{E}, \qquad \nabla \cdot \vec{H} = 0 \tag{4}$$

since the permeability is unity for all materials at optical frequencies. Thus the physical properties of the medium are characterized by the values of the dielectric constant ϵ, and the conductivity σ. In a simple model, polarization effects in a non-conducting medium may be attributed to the atomic polarizations of the constituent atoms. Then ϵ is given by

$$\epsilon = 1 + 4\pi n_o \alpha \tag{5}$$

where n_o is the number of atoms per unit volume, and α is the atomic polarizability of a single atom. The results of more realistic calculations can usually be put into a similar form. Then, if one assumes that the time variation of the electromagnetic field is $\exp(-i\omega t)$, ω being the circular frequency of the wave, one gets from the Equations (4) and (5)

$$\nabla \times \vec{H} = (1 + 4\pi n_o \alpha + i\frac{4\pi\sigma}{\omega})\frac{1}{c}\frac{\partial \vec{E}}{\partial t}$$

or

$$\nabla \times \vec{H} = \frac{\tilde{\epsilon}}{c}\frac{\partial \vec{E}}{\partial t} \tag{6}$$

where

$$\tilde{\epsilon} = \epsilon_1 + i\epsilon_2 \tag{7}$$

is the complex dielectric constant. The real part of the complex dielectric constant

$$\epsilon_1 = 1 + 4\pi n_o \alpha \tag{8}$$

gives the polarizability of the medium, while the imaginary part

$$\epsilon_2 = \frac{4\pi\sigma}{\omega} \tag{9}$$

is related to the rate of absorption of energy by the medium. Eliminating $\vec{H}$ in Equation (4), one obtains

$$\nabla^2 \vec{E} = \frac{\epsilon_1}{c^2} \frac{\partial^2 \vec{E}}{\partial t^2} + \frac{4\pi\sigma}{c^2} \frac{\partial \vec{E}}{\partial t} , \tag{10}$$

which has a solution of the form

$$\vec{E} = \vec{E}_o \exp[i(\vec{K} \cdot \vec{r} - \omega t)], \tag{11}$$

where

$$|\vec{K}| = \frac{\omega}{c} \left| \sqrt{\tilde{\epsilon}} \right| \tag{12}$$

is the dispersion relation of the electromagnetic wave in a dispersive medium.

Comparing Equations (3) and (11), one obtains

$$\tilde{n} = n + ik = \sqrt{\tilde{\epsilon}} \ . \tag{13}$$

The real and imaginary parts of $\tilde{n}$ and $\tilde{\epsilon}$ are related by

$$\epsilon_1 = n^2 - k^2 \qquad \text{(polarization behavior)} \tag{14}$$

$$\epsilon_2 = 2nk \qquad \text{(absorption behavior)} . \tag{15}$$

II. OPTICAL PROPERTIES

The interaction of light with a solid may be described in terms of the parameter $\tilde{\epsilon}$. The goal of theory is to calculate $\tilde{\epsilon}$ as a function of ω assuming some microscopic model. Results calculated with two models are given in this section. Drude's free-electron model of metallic structure accounts for the qualitative optical behavior of the alkali metals such as high reflectivity at visible frequencies and transparency in the ultraviolet. Calculations based on an independent-particle quantum mechanical model are then described which account for many of the observed deviations from free electron behavior.

Classical Free Electron Theory

A classical treatment of the optical properties of metals, based on the assumption of perfectly free electrons, was developed by Drude (1900, 1904), Zener (1933), and Kronig (1933, 1934). In Drude's model the valence electrons are treated as free particles moving in a time-varying electric field and subject to a velocity-dependent damping force. The classical equation of motion for the x-component of the displacement of the particle is

$$m \frac{\partial^2 x(z,t)}{\partial t^2} = -e E_x(z,t) - 2\pi m \gamma \frac{\partial x(z,t)}{\partial t} \tag{16}$$

where $-e$ and m are, respectively, the charge and mass of the electron, γ is the damping constant, and $E_x(z,t)$ is the time varying electric intensity

(propagating in the z-direction) given by Equation (3). The stationary solution of the form, $x(z, t) = x_o(z)e^{-i\omega t}$, is

$$x(z, t) = \frac{e/m}{\omega^2 + i2\pi\gamma\omega} E_x(z, t) . \tag{17}$$

The complex polarization $P_x(z, t)$ is related to the electric intensity $E_x(z, t)$ according to the equation

$$P_x(z, t) = \frac{\tilde{\epsilon} - 1}{4\pi} E_x(z, t) . \tag{18}$$

The polarization is also defined as follows:

$$P_x(z, t) = - n_c e x(z, t) \tag{19}$$

where n_c is the number of conduction electrons per unit volume. With the definition of the complex dielectric constant given by Equation (7), substitution of Equations (18) and (19) into Equation (17) gives

$$\epsilon_1 = 1 - \frac{\omega_o^2}{\omega^2 + (2\pi\gamma)^2} \tag{20}$$

and

$$\epsilon_2 = 2\pi\gamma \frac{\omega_o^2}{\omega[\omega^2 + (2\pi\gamma)^2]} \tag{21}$$

where

$$\omega_o^2 = \frac{4\pi n_c e^2}{m} . \tag{22}$$

The value of $2\pi\gamma\hbar$, estimated from the static conductivity of cesium [Mott and Jones (1936)] is .028 eV. Thus, for photon energies much greater than .028 eV, Equations (20) and (21) become

$$\epsilon_1 = 1 - \frac{\omega_o^2}{\omega^2} \tag{23}$$

and

$$\epsilon_2 = 2\pi\gamma \frac{\omega_o^2}{\omega^3} . \tag{24}$$

The behavior of ϵ_1 and ϵ_2 for a free electron as a function of ω is shown in Figure 1.

Wood (1933a, b) observed that cesium films were highly transparent to photons of wavelengths shorter than 4400 Å (2.82 eV) and highly reflecting for photons of longer wavelengths. Zener (1933) showed that Wood's observation could be explained by the classical theory if the conduction electrons were treated as free, that is, the damping constant is zero. In this case Equations (23) and (24) become

$$\epsilon_1 = n^2 - k^2 = 1 - \frac{\omega_o^2}{\omega^2} , \tag{25}$$

$$\epsilon_2 = 2nk = 2\pi\gamma \frac{\omega_o^2}{\omega^3} = 0, \tag{26}$$

or

$$nk = 0 . \tag{27}$$

There is a critical frequency ω_o when ϵ_1 is zero, that is, at

$$\omega_o^2 = \frac{4\pi n_c e^2}{m} . \tag{28}$$

A calculation gives the critical wavelength for cesium as 3600 Å (3.42 eV). The frequency ω_o, called the free-electron plasma frequency, is the

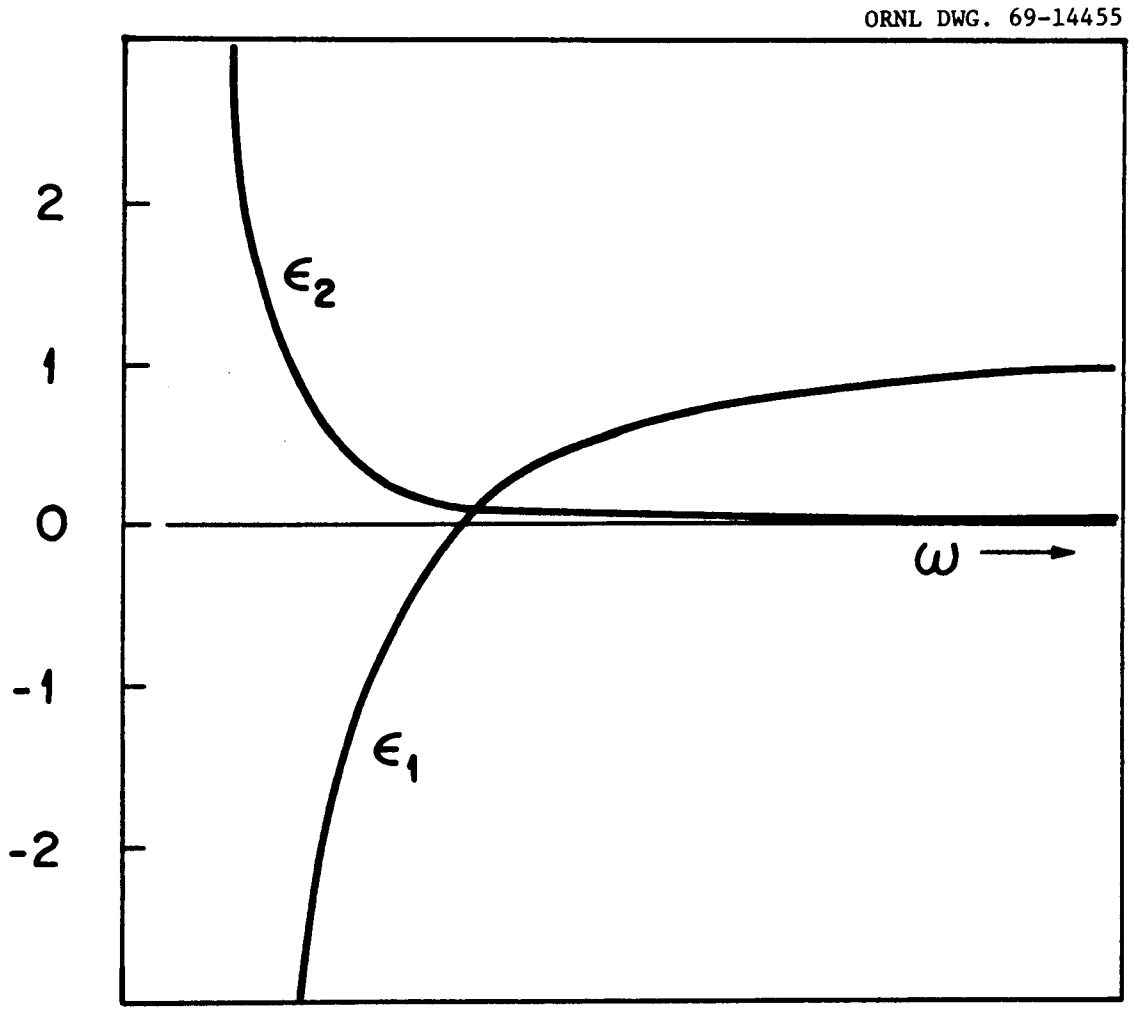

Figure 1. Behavior of ϵ_1 and ϵ_2 as a function of ω for free electrons.

frequency separating the high frequency spectral regions in which the material is transparent from the low frequency region in which it is reflecting. Equations (26) and (27) show that $k = 0$ for $\omega > \omega_o$, or $\lambda < \lambda_o$, while $n = 0$ for $\lambda > \lambda_o$ since n and k are both real numbers. When $\lambda > \lambda_o$, the radiation is totally reflected, and when $\lambda < \lambda_o$ a portion of the radiation is reflected. These arguments are obvious from the relation for the normal incidence reflectance R of the radiation incident on a matter from vacuum:

$$R = \frac{(n_{rel} - 1)^2 + k_{rel}^2}{(n_{rel} + 1)^2 + k_{rel}^2} \tag{29}$$

which gives $R = 1$ for $n = 0$, that is, all incident radiation is reflected.

In the absence of interband transitions, Cohen's quantum mechanical treatment of the following section gives equations of the same form as Equations (20) through (22). The effects of a periodic lattice appear in two ways. The free electron mass is replaced by an effective mass m_{eff}, and γ is calculated explicitly from the electron-photon interactions in a metal. Some authors in comparing experimental results to theory have treated the electron density as an adjustable parameter rather than the effective mass. Then n_{eff} replaces n_c and m is retained as a free electron mass.

Drude (1900) and Lorentz (1909) also applied the simple theory to dielectrics by assuming that the electrons were bound rather than free. It was assumed that the dielectric contained n_c bound electrons per unit volume, each electron obeying a differential equation,

$$m \frac{\partial^2 \vec{x}}{\partial t^2} = -e\vec{E} - m\omega_r^2 \vec{x} - 2\pi\gamma m \frac{\partial \vec{x}}{\partial t} . \tag{30}$$

the new term is $-m\omega_r^2 \vec{x}$, where ω_r is the resonant frequency, describing a restoring force proportional to displacement. The solution is

$$\vec{x} = \frac{-(e/m)\vec{E}}{(\omega_r^2 - \omega^2) + i(2\pi\gamma\omega)^2} . \tag{31}$$

Calculating the dielectric constant as before, we find that

$$\tilde{\epsilon} = 1 + \frac{(4\pi n_c e^2/m)}{\omega_r^2 - \omega^2 - i2\pi\gamma\omega} \tag{32}$$

or

$$\epsilon_1 = 1 + \frac{\omega_o^2}{(\omega_r^2 - \omega^2) + (4\pi\gamma\omega)^2/(\omega_r^2 - \omega^2)} \tag{33a}$$

and

$$\epsilon_2 = \frac{2\pi\gamma\omega_o^2\omega}{(\omega_r^2 - \omega^2) + (2\pi\gamma\omega)^2} . \tag{33b}$$

When plotted, $\epsilon_1 - 1$ and $\omega\epsilon_2$ have the form shown in Figure 2. Several features of these curves are of interest when $2\pi\gamma \ll \omega$ and $\omega \ll \omega_r$. ϵ_1 is increased by the existence of a strong resonance at higher energy. A similar effect is obtained in more realistic calculations. ϵ_2 has a maximum near ω_r, indicating optical absorption near resonant frequencies.

The model can be generalized by assuming that n_r of the n_c oscillator have the frequency ω_r. We define an oscillator strength $f_r = n_r/n_c$ which means the relative strength at the various absorption frequencies,

ORNL DWG. 69-14452

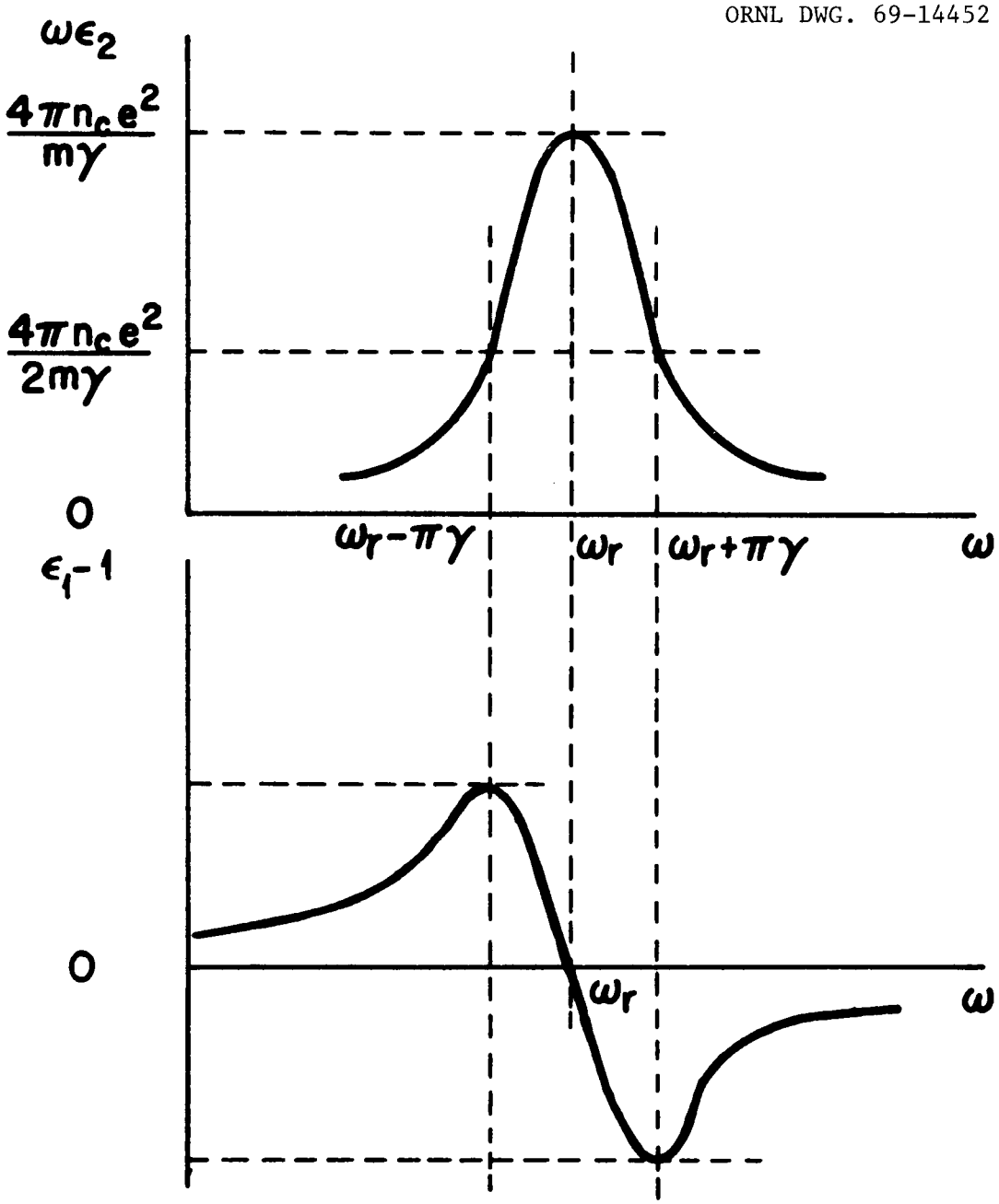

Figure 2. Dependence of $\epsilon_1 - 1$ and $\omega\epsilon_2$ on frequency.

and obtain

$$\tilde{\epsilon} = 1 + \sum_r \frac{f_r \omega_o^2}{\omega_r^2 - \omega^2 - i2\pi\gamma_r \omega} \tag{34}$$

and

$$\sum_r f_r = 1 . \tag{35}$$

The results of the quantum mechanical calculations of the following section can be put in a form very similar to Equation (34). In that theory $\hbar\omega_r$ is the energy difference between filled and empty states at a position r in the Brillouin zone, and f_r gives a measure of the strength of the transition matrix elements connecting the initial and final states. A condition similar to Equation (35) applies to the sum of all oscillator strengths in the quantum mechanical treatment.

In this thesis, measurements of optical constants are reported which lie at frequencies above ω_o, the plasma frequency. As indicated in Figure 1, page 13, the optical absorption (which is proportional to ϵ_2) due to free carrier absorption is small in this region and ϵ_1 approaches +1. Under these conditions, the model predicts that a free electron gas becomes transparent with an index of refraction $n \simeq 1$ and very small residual absorption.

Qualitatively similar behavior is observed in all of the alkali metals, but quantitatively they differ in two major respects. The absorption is larger than that associated with free carrier absorption and ϵ_1 is greater than + 1. These two effects can be partially understood on the basis of a quantum

mechanical treatment of direct transition leading to an equation similar to Equation (34). The results of such a calculation are described below. It seems probable that in cesium, interband transitions between one electron states do not serve to account for all of the observed absorption in the ultraviolet, and that collective effects must be involved to explain the observed absorption. These effects are discussed in a later section.

Quantum Mechanical Theory

The wave functions of the outer electrons of the atom overlap to form bands because of the close proximity of atoms in a solid, and the outer electrons are free to diffuse through the volume of the solid. Thus, the properties of the outer electrons approximate those of a free electron gas, and the collective response of these electrons subject to an electromagnetic radiation field can be treated with quantum mechanical rigor.

The quantum mechanical description of the optical properties of metals is based on an independent-particle model [Seitz (1940), Fröhlich (1936), Cohen (1958)]; that is, each electron of the solid is acted upon by a fixed potential function which includes the effects of the atomic nuclei and the average effect of all of the remaining electrons. According to this model, if the local field corrections are neglected, the results of the dielectric constant calculation in a cubic metal for light of angular frequency ω are

$$\epsilon_1 = 1 - \frac{4\pi e^2}{m\omega^2} \sum_j \frac{2}{(2\pi)^3} \int d^3\vec{k}\, f_{j\vec{k},j\vec{k}} - \frac{4\pi e^2}{m} \sum_{j\neq i} \frac{2}{(2\pi)^3} \int d^3\vec{k} \sum_i \frac{f_{i\vec{k},j\vec{k}}}{\omega^2 - \omega^2_{i\vec{k},j\vec{k}}} \tag{36}$$

and

$$\epsilon_2 = \frac{2\pi^2 e^2}{m\omega^2} \sum_{j\neq i} \frac{2}{(2\pi)^3} \int d^3\vec{k} \sum_i |f_{i\vec{k},j\vec{k}}|\, \delta(\omega_{i\vec{k},j\vec{k}} - \omega) \tag{37}$$

where $\vec{k}$ is the wave vector of an electron, $f_{i\vec{k},j\vec{k}'}$ is the average oscillator-strength density for a transition from state $\vec{k}'$ in filled band j to a state $\vec{k}$ in unfilled band i, and $\omega_{i\vec{k},j\vec{k}}$ is related to the difference in energy between the states by

$$\omega_{i\vec{k},j\vec{k}} = \frac{\epsilon_{i\vec{k}} - \epsilon_{j\vec{k}}}{\hbar}, \tag{38}$$

$\hbar$ being Planck's constant divided by 2π. The delta function in the expression ϵ_2 insures the conservation of energy. At optical frequencies the momentum of the photon is much less than the momentum of an electron in the crystal. Therefore, for optically induced interband transitions in which phonons are not involved the crystal momentum is essentially unchanged, i.e., $\vec{k} \simeq \vec{k}'$. Thus, direct or vertical interband transitions occur as illustrated in Figure 3 which shows the calculated energy values of the electronic states of metallic cesium [Kenney (1967), Ham (1962), Callaway (1957), Mahanti and Das (1969)] as a function of $\vec{k}$ along a Σ-axis between the origin and the Brillouin zone boundary (reduced zone scheme).

ORNL DWG. 69-14454

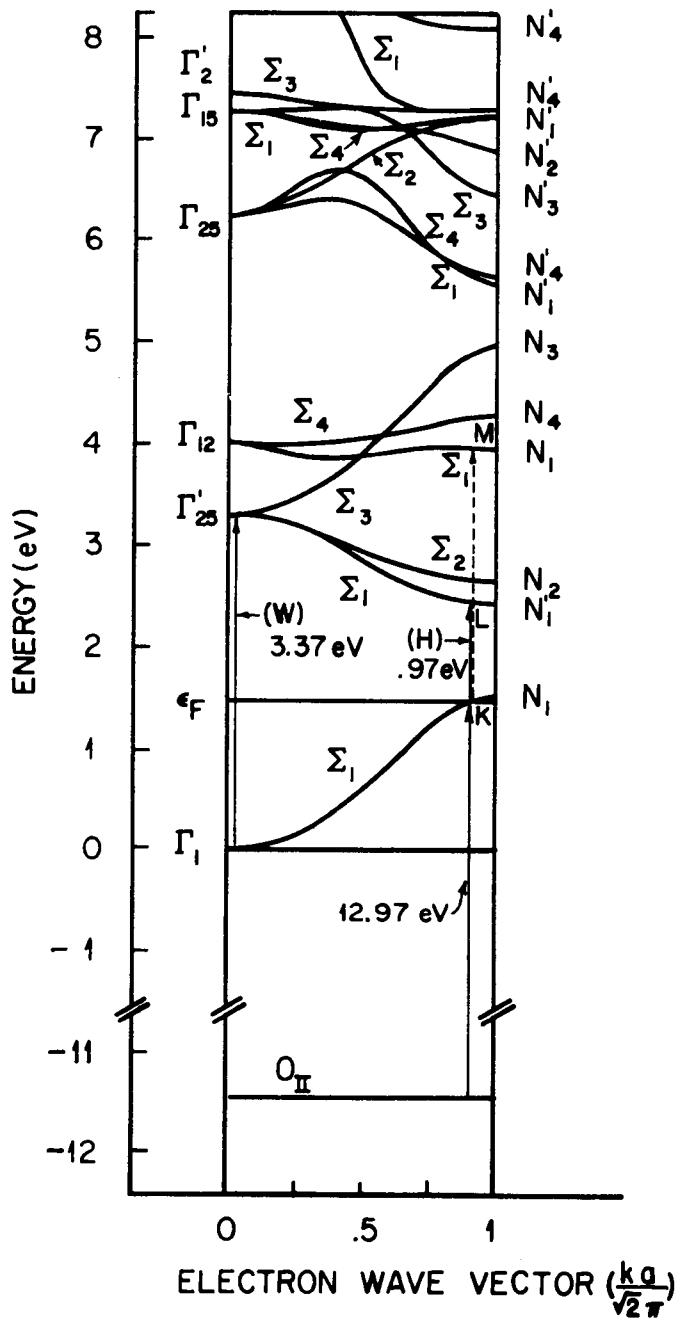

Figure 3. Energy bands of cesium along a (1, 1, 0) axis.

The average oscillator strength for an interband transition is a function of the momentum-matrix elements connecting the initial and the final states, and of the energy difference between the states:

$$f_{i\vec{k},j\vec{k}} = \frac{2}{3m} \frac{\langle i\vec{k}|\vec{p}|j\vec{k}\rangle \cdot \langle j\vec{k}|\vec{p}|i\vec{k}\rangle}{\epsilon_{i\vec{k}} - \epsilon_{j\vec{k}}} . \tag{39}$$

The average oscillator strength inserted in the second term of Equation (36) is the one connecting a state in a filled band with itself and is given by

$$f_{j\vec{k},j\vec{k}} = \frac{m}{3\hbar^2} \nabla^2_{\vec{k}} \epsilon_{j\vec{k}} . \tag{40}$$

The summation terms in Equations (36) and (37) represent the contributions from interband transitions. That is, the sum over i includes all states of wave number $\vec{k}$ which are initially empty, and the sum over j includes all partially or fully occupied states, that is, we have $\epsilon_i > \epsilon_F$ and $\epsilon_j \leq \epsilon_F$, with ϵ_F being the Fermi level, in both Equations (36) and (37). The $\vec{k}$-integration is over the occupied region of the jth band. In general, $f_{j\vec{k},j\vec{k}}$ must be summed over all occupied states. However, the highest core level of cesium (0_{II} in Figure 3) [Bearden and Burr (1965)] lies 11.4 eV below the bottom of the conduction band and is practically independent of $\vec{k}$ as are the other core bands which lie further below the conduction band and, therefore, $f_{j\vec{k},j\vec{k}}$ is equal to zero. Thus, for cesium the summation over j in the second term in Equation (36) is suppressed and the subscript j in $f_{j\vec{k},j\vec{k}}$ is replaced by c which represents the conduction band only. In the third term in Equation (36)

the band index c should appear in both $\sum_j$ and $\sum_i$ since the conduction band contains both filled and empty states. The $\vec{k}$-integration in Equations (36) and (37) is over the occupied region of the jth band, which is now understood as the conduction band c for cesium. Since the second term in Equation (36) is affected only by the filled states of the conduction band, the integration is restricted to $\vec{k}$ inside the Fermi surface. The oscillator strengths are independent of spin and thus the result of summation over spin states is included in the equations by the factor two.

The second term in Equation (36) is the sum of contributions of static displacements of charge in each band [of which only the conduction band is important, as $f_{j\vec{k},j\vec{k}} \simeq (\partial^2 E_{j\vec{k}})/(\partial k\, \partial k) \simeq 0$ for other than the conduction band]. The third term is from the dipole moment due to the transition charge density associated with states $|i\vec{k}\rangle$ and $|j\vec{k}\rangle$ which satisfy conservation of energy and crystal momentum.

An averaged effective mass of the conduction electrons, m_{eff}, is defined such that m/m_{eff} is the average value of the conduction band oscillator strength, $f_{c\vec{k},c\vec{k}}$:

$$\left(\frac{m}{m_{eff}}\right)_c = \frac{2}{(2\pi)^3}\,\frac{1}{n_c}\int d^3\vec{k}\, f_{c\vec{k},c\vec{k}}\,, \tag{41}$$

where the integration is over the occupied region of the conduction band. In general, for metals m is less than m_{eff}.

With the definition of an effective mass, Equation (36) can be put in a form similar to Equation (23):

$$\epsilon_1 = 1 - \frac{\omega_a^2}{\omega^2} + \delta\epsilon_1(\omega), \tag{42}$$

where

$$\omega_a^2 = \frac{4\pi n_c e^2}{m_{eff}} \tag{43}$$

and $\delta\epsilon_1(\omega)$ is the contribution of interband transitions and of static displacements of charge in other bands than the conduction band. ϵ_2 arises entirely from the absorption of radiation via interband transitions which occur when ω equals $\omega_{i\vec{k},j\vec{k}}$. According to Cohen's (1958) theory, two simple approximations are possible: (1) If photon energies are sufficiently less than the interband absorption edge, that is, ω^2 much less than any $\omega^2_{i\vec{k},j\vec{k}}$, $\delta\epsilon_1(\omega)$ is very nearly constant, and Equation (42) simplifies to

$$\epsilon_1 = 1 + 4\pi n_o \alpha_T - \frac{\omega_a^2}{\omega^2}, \quad (\text{for } \omega \ll \omega_{i\vec{k},j\vec{k}}) \tag{44}$$

where

$$\alpha_T = \frac{e^2}{mn_o} \sum_{j \neq i} \frac{2}{(2\pi)^3} \int d^3\vec{k} \sum_i \frac{f_{i\vec{k},j\vec{k}}}{\omega^2_{i\vec{k},j\vec{k}}} \tag{45}$$

is the total polarizability of an atom in the crystal lattice, and n_o is the number of atoms per unit volume. The lowest energy required for interband transition in cesium is .967 eV, which is labeled as (H) in Figure 3, page 20. This transition occurs from states just below the Fermi energy in the conduction band with wave vector along a Σ-axis to states with the same wave

vectors in the first unoccupied band. Equation (44) should be valid for energies greater than .028 eV but less than .967 eV according to the independent-particle model. (2) If interband absorption occurs, but the absorption frequencies are spread over a sufficiently wide range of energy, and if the corresponding oscillator strengths are not strongly energy dependent, an approximation for $\delta\epsilon_1(\omega)$ could be considered as follows: (a) A sum over transitions from core bands to unfilled bands, (b) a sum over transitions from the conduction bands to unfilled bands for which $\omega_{i\vec{k},c\vec{k}} > \omega$, and (c) a sum over conduction band transitions for which $\omega_{i\vec{k},c\vec{k}} < \omega$. For the terms (a) and (b) the energy denominator $\omega^2 - \omega^2_{i\vec{k},c\vec{k}}$ is replaced by $-\omega^2_{i\vec{k},c\vec{k}}$ and for the term (c) by ω^2. [This approximation is good if those k for which $\omega^* \simeq \omega$ give a relatively small contribution to ϵ_1, as occurs when ω^* has a wide spread of values, $\omega^*(k)$ being the minimum optical excitation energy for a conduction electron of wave number k.] Then Equation (36) becomes

$$\epsilon_1 = 1 + 4\pi n_o \alpha_o + \frac{4\pi e^2}{m} \sum_{\substack{\omega_{i\vec{k},j\vec{k}} > \omega \\ i \\ (j = c)}} \frac{2}{(2\pi)^3} \int d^3\vec{k} \, \frac{f_{i\vec{k},c\vec{k}}}{\omega^2_{i\vec{k},c\vec{k}}}$$

$$- \frac{\omega_a^2}{\omega^2} - \frac{4\pi e^2}{m\omega^2} \sum_{\substack{\omega_{i\vec{k},j\vec{k}} < \omega \\ i \\ (j = c)}} \frac{2}{(2\pi)^3} \int d^3\vec{k} \, f_{i\vec{k},c\vec{k}} \qquad (46)$$

where

$$\alpha_o = \frac{e^2}{mn_o} \sum_{j \neq c} \frac{2}{(2\pi)^3} \int d^3\vec{k} \sum_i \frac{f_{i\vec{k},j\vec{k}}}{\omega^2_{i\vec{k},j\vec{k}}} \tag{47}$$

is the contribution of the core bands to α_T. When the spread in values of the minimum optical excitation energy for conduction electron is sufficiently large, the third term in Equation (46) depends only slightly on ω, and the fifth term depends on ω nearly as ω^{-2}. Combinations of similar terms give

$$\epsilon_1 = 1 + 4\pi n_o \alpha_1 - \frac{\omega_b^2}{\omega^2} \tag{48}$$

where the definitions of α_1 and ω_b become apparent upon comparison of Equations (46) and (48). An optical effective mass of electron, m_{opt}, can be defined in both cases (1) and (2), in analogy with expression (43),

$$\omega_b^2 = \frac{4\pi n_c e^2}{m_{opt}} \quad . \tag{49}$$

Comparison of Equations (44), (46), and (48) shows that

$$m_{opt} \leq m_{eff} \tag{50}$$

where equal sign is for the case (1), and also

$$\alpha_T \geq \alpha_1 \geq \alpha_o \; . \tag{51}$$

If $m_{eff} = m_{opt} = m$, the first two terms in Equation (42) and the first and third terms in Equation (48) are essentially the results of the free electron

theory given by Equation (23). Equation (48) is valid if the range of energies for transitions from filled band in the conduction band to empty states in higher band is large. The threshold for these transitions is .967 eV corresponding to transition (H) in Figure 3, page 20. The highest energy transition between the conduction band and the first unoccupied band occurs at Γ and has an energy 3.37 eV, labeled (W) in Figure 3. Transitions from the conduction band to unoccupied higher bands continue without interruption, starting from 1.17 eV to photon energies greater than the threshold for the excitation of core electrons which is 11.4 eV. Equation (48) is applicable for photon energies from .967 eV to near 11.4 eV.

III. REFLECTANCE AND TRANSMITTANCE OF LIGHT AT NON-NORMAL INCIDENCE

Considering a plane wave incident on the vacuum interface of the infinitely thick absorbing medium characterized by the complex refractive index $\tilde{n} = n + ik$, the Fresnel coefficients of refraction and transmission are defined as follows [Born and Wolf (1965)]:

$$r_p = \frac{\cos\theta_r - \tilde{n}\cos\theta_i}{\cos\theta_r + \tilde{n}\cos\theta_i} ,$$

$$r_s = \frac{\cos\theta_i - \tilde{n}\cos\theta_r}{\cos\theta_i + \tilde{n}\cos\theta_r} , \qquad (52)$$

and

$$t_p = \frac{2 \cos \theta_i}{\cos \theta_r + \tilde{n} \cos \theta_i} ,$$

$$t_s = \frac{2 \cos \theta_i}{\cos \theta_i + \tilde{n} \cos \theta_r} \tag{53}$$

where r_p and r_s are the coefficients of the parallel- and perpendicular-polarized component of reflected radiation, respectively; t_p and t_s are the similar components of transmitted radiation; θ_i and θ_r are the angles of incidence and reflection, respectively. Snell's law gives the relation between the parameters θ_i, θ_r, and $\tilde{n}$. For our case the law is given by

$$\sin \theta_i = \tilde{n} \sin \theta_r . \tag{54}$$

Thus, the components of the reflectances in terms of θ_i and $\tilde{n}$ can be written as

$$R_p = \left| \frac{\sqrt{\tilde{n}^2 - \sin^2 \theta_i} - \tilde{n}^2 \cos \theta_i}{\sqrt{\tilde{n}^2 - \sin^2 \theta_i} + \tilde{n}^2 \cos \theta_i} \right|^2 \tag{55}$$

and

$$R_s = \left| \frac{\sqrt{\tilde{n}^2 - \sin^2 \theta_i} - \cos \theta_i}{\sqrt{\tilde{n}^2 - \sin^2 \theta_i} + \cos \theta_i} \right|^2 \tag{56}$$

For partially plane polarized light the total reflectance of the surface is

$$R = \frac{R_s + P R_p}{1 + P} \tag{57}$$

where P is the ratio of the intensities of the incident radiation polarized parallel, I_p, and perpendicular, I_s, to the plane of incidence,

$$P = \frac{I_p}{I_s} . \tag{58}$$

CHAPTER IV

EXPERIMENTAL APPARATUS

The primary components of the experimental system are a light source, a monochromator, a reflectance chamber, a photomultiplier detector, and associated electronics.

These components are shown schematically in Figure 4. Light produced by a high voltage gas discharge passes into the monochromator through the entrance slit and filter assembly and is incident on the concave grating. Monochromatic light from the grating passes through the exit slit into the reflectance chamber and onto the evaporated film. Its reflectance is measured as a function of angle of incidence by a photomultiplier tube which may be rotated about the vertical axis of the sample.

Wavelengths used in this experiment ranged from about 1200 Å (10 eV) to 5000 Å (2.5 eV). The hydrogen line spectrum was used for wavelengths from 1200 Å to 1670 Å, and the line spectrum of air between 1600 Å and 5000 Å. Both types of spectra are excited by a d. c. discharge.

The capillary discharge light source has been described elsewhere [Sutherland (1967), Hayes (1968), Painter (1968)]. The light intensity of radiation is very sensitive to the pressure in the capillary tube. Thus, care has to be taken to maintain a constant pressure within the light source. The operating pressure was 2 Torr for air and 20 Torr for hydrogen, and the operating current was 250 mA through a 5/32 inch diameter capillary.

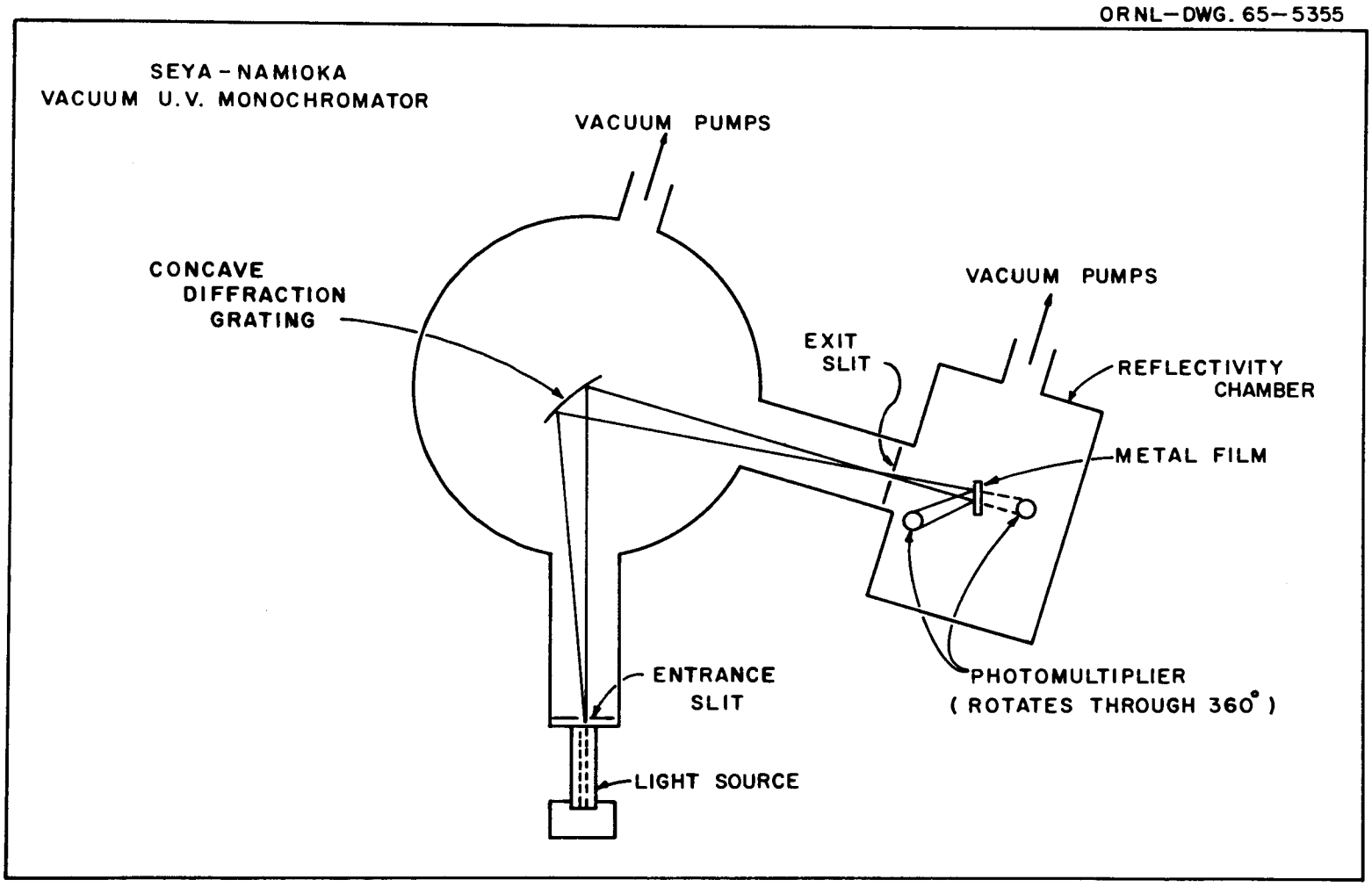

Figure 4. Schematic diagram of apparatus.

The light source is isolated from the chamber by one of a set of filters. Filters of lithium fluoride (LiF), quartz, and glass are mounted behind the light source and the entrance slit assembly. They are used to distinguish between first and second order spectra from the grating and also to help determine the intensity of background radiation. LiF transmits at wavelength above 1050 Å, quartz above 1550 Å, and glass above 2800 Å.

The Seya-Namioka type vacuum scanning monochromator system was available at the Oak Ridge National Laboratory (ORNL) to accommodate a concave diffraction grating of a radius of curvature of 50 cm. The optical design is similar to that of the McPherson 50 cm Seya instrument. Entrance and exit slits are set 70.5° apart. These bilateral slits are continuously adjustable from a closed position to 6 mm by means of a micrometer screw attached directly to the slit assembly. A vacuum-tight slide valve is located on each slit assembly and is used to isolate the slits from the evacuated chamber.

Light is dispersed by a gold-coated Jarrell-Ash concave grating ruled with 1180 lines per millimeter with a reciprocal dispersion at the exit slit of about 14 Å per millimeter. Slits were normally operated at .250 mm giving an output line width of 3.5 Å.

A small magnet is placed between the light source and entrance slit to sweep any charged gas particles out of the optical path.

The chamber used for preparing cesium films and measuring the reflectance of the films is shown in Figure 5. It is a stainless steel cylinder 16 inches long and 8.5 inches in diameter with four ports arranged as a cross on the lower half of the chamber. One is connected to the exit slit of the monochromator and a second to a cold-water-trapped diffusion pump. The remaining two are used as view ports. The sample holder assembly, high current feed-throughs, and baffles are mounted on the top flange of the chamber. The rotating photomultiplier (PM) tube detector is mounted on the bottom flange of the chamber. All vacuum seals are made with Viton O-rings.

The sample substrate, in our case a quartz or calcium fluoride semicylinder, may be rotated through 360°. Cesium was evaporated onto the substrate from a tantalum boat.

The PM tube, type RCA 1P21, was coated with sodium salicylate and operated at 500 or 600 volts. The photocurrent was measured by a Keithley model 409 pico-ammeter and recorded by a Minneapolis-Honeywell Brown 10-millivolt strip chart recorder.

The angle-doubling mechanism is shown schematically in Figure 5. The photomultiplier and sample holder are connected by a belt and pulley mechanism that rotates the phototube through twice the angle of the sample, and thus keeps the phototube in the reflected beam. The shafts which support the photomultiplier and sample holder are connected to an external shaft by toothed nylon belts and associated toothed pulleys. The

ORNL-DWG 69-12856

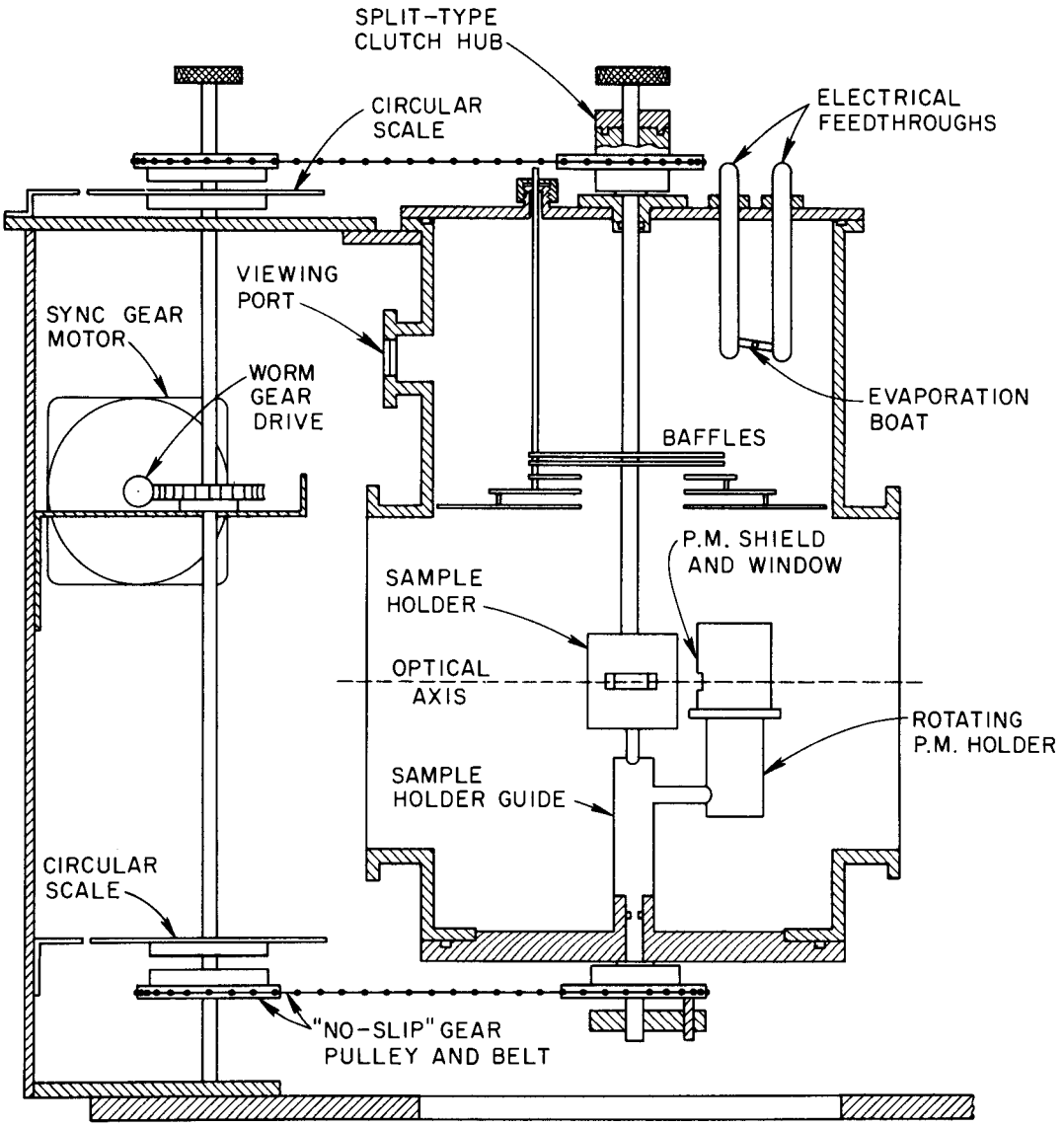

Figure 5. Schematic diagram of reflectance chamber and angle doubler.

shaft of the sample holder is connected to its pulley by a split type clutch hub to facilitate withdrawal of the sample from the beam. The external shaft is driven by a five-speed synchronous motor. There was no significant backlash in the assembly.

The calcium fluoride (CaF_2) semicylinder used in this experiment is shown in Figure 6. Cesium metal was evaporated on the upper half of the semicylinder only so that one could measure reflectances from both the semicylinder-cesium and semicylinder-vacuum interfaces under the same vacuum pressure and the same radiation intensities. Since the sample holder was movable vertically, both measurements could be made by raising or lowering the shaft.

The CaF_2 used in this experiment was transparent to photons of wavelengths greater than 1300 Å.

In this experiment we wished to measure the reflectance of unoxidized cesium surfaces. Consequently, the measurements were made at the substrate-cesium interface rather than on the free surface side. The technique and advantages of the use of the semicylinder have been discussed in detail by Sutherland et al. (1968). The semicylindrical shape insures that the incident and reflected beams are always normal to the curved substrate-vacuum interface.

The reflectance chamber is connected to a National Research Corporation (NRC) water-cooled baffle, a NRC slide valve, and a 6-inch, water-cooled oil diffusion pump, NRC model HS6-1500, with pumping speed

ORNL DWG. 67-6716R

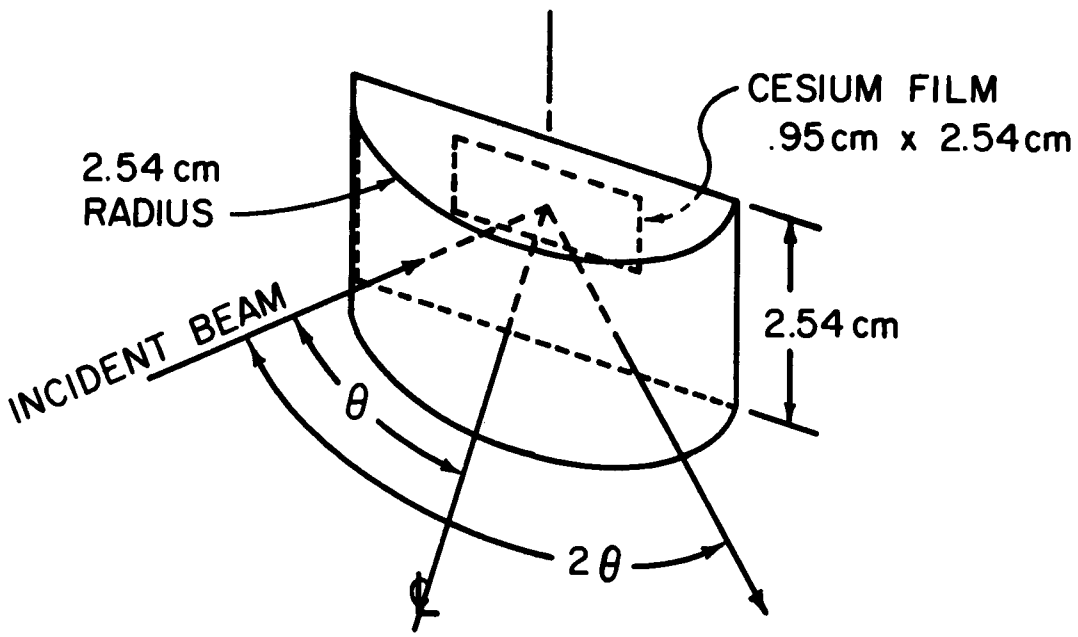

Figure 6. Diagram of semicylinder.

of 1400 liters per second at 10^{-6} Torr. The system is backed by a 15 cubic feet per minute Welch model 1397 forepump. Pressure in the reflectance chamber is measured by a Veeco RG 75K ionization gauge tube and read on a Vactronic ion gauge control SP-230. The monochromator is evacuated by a NRC VHS6 water-cooled oil diffusion pump with a pumping speed of 2400 liters per second at 10^{-6} Torr. The reflectance chamber can be isolated by a slide valve incorporated in the exit-slit assembly of the monochromator. The pressure in the reflectance chamber can be reduced to about 1.5×10^{-6} Torr by pumping out for about a half day, and the liquid nitrogen cold trap which is mounted on an elbow flange can reduce the pressure to less than 3×10^{-7} Torr within an hour.

CHAPTER V

EXPERIMENTAL PROCEDURE

The basic measurements used for determining the optical properties of cesium metal in the vacuum ultraviolet are simple if one ignores the problems associated with light source instabilities, vacuum system limitations, sample quality, weak information signals, and background effects, among less obvious difficulties that arise. In a word, proficiency is required in areas such as the preparation of evaporated film samples and optical reflectivity measurements in the vacuum ultraviolet region. Some major and minor technical problems required in this experiment are discussed in the following.

I. ALIGNMENT OF THE OPTICAL SYSTEM

In the measurements of reflectivity as a function of angle θ, the sample and detector must be rotated through angles of θ and 2θ, respectively, with respect to the incident beam. Very careful optical alignment is required to keep the reflected beam centered on the detector throughout the full rotation. Visual alignment at atmospheric pressure was accomplished using the zero order beam from the unevacuated vacuum monochromator. At normal incidence, the area of the sample illuminated by the beam was about 3 mm x 5 mm. Alignment was satisfactory when the illuminated area increased symmetrically in width as the sample was rotated

away from normal incidence and the beam remained centered on the detector. A further check was made after the chamber was evacuated by measuring the reflectivity of a known interface. For this purpose, the critical angle curve for the substrate-vacuum interface was normally used.

The wavelength counter of the vacuum monochromator was calibrated using mercury spectral lines. The resulting calibration was accurate to about 1 Å.

II. PREPARATION OF CESIUM FILM

The semicylinder substrate was initially masked on both flat and curved surfaces with teflon tape. Before evaporation the cesium was degassed for 5 to 10 minutes by gentle heating. The evaporation rate was then increased and the flat surface of the semicylinder exposed by stripping the tape from this surface. Following evaporations of 8 to 60 seconds, the remaining tape was stripped from the curved surface for measurements. The photomultiplier tube detector was also masked during the evaporation.

The system pressures during the evaporation were 1.5 to 2×10^{-7} Torr before evaporation, 6 to 10×10^{-7} Torr during degassing, 4 to 5×10^{-6} Torr during evaporation, and 4 to 5×10^{-7} Torr shortly after the evaporation. The best films as judged by color (gold tint) and stability of optical constants with time after evaporation were those formed in 10 seconds or less.

The evaporation boats were loaded with about 300 mg of 99.97% pure cesium. The cesium was transferred to the boats from glass storage

ampules in a glove box filled with argon. They were then stored in an argon atmosphere until ready for use, and loaded into an argon filled experimental chamber.

III. REFLECTANCE MEASUREMENTS

The procedures were designed to minimize the interval between formation of the film and the beginning of the reflectance measurements.

The measuring system was checked out and ready to start measurements prior to evaporation; that is, a stable discharge was turned on, the wavelength scale of the monochromator was set to an intense line, and the leakage of light into the chamber was checked by turning off the lights in the room, while monitoring the photomultiplier output current. The minimum time between evaporation and the first measurement of the reflectance was about five minutes. The maximum intensity of each spectral line was obtained by manually adjusting the wavelength scale while observing the output of the photomultiplier.

The motor-driven angle doubler was used to measure reflectance as a function of incident angle. The photomultiplier blocked the incident radiation from angles of incidence less than about 13°, while for angles greater than 78° the sample holder obstructed the beam.

The relation

$$R(\theta) = \frac{I(\theta)}{I_o} \tag{59}$$

gives the reflectance $R(\theta)$ of the substrate-cesium surface when $I(\theta)$ is the intensity of radiation reflected from the substrate-cesium interface and I_o is the intensity of the substrate-vacuum interface for angles greater than the critical angle.

IV. DETERMINATION OF BACKGROUND

The background intensity of the detection system was primarily due to scattered light of other wavelength and to the dark current of the photomultiplier. To determine reflectance due to radiation of the desired wavelength, the background effect must be subtracted from the direct reflectance readings.

The background intensity when the light source was operated with d.c. excitation was constant above 500 Å for a given photomultiplier position. The background was determined by observing the response of the photomultiplier detector when the wavelength scale of the monochromator was set to 800 Å, since a d.c. discharge in hydrogen or air produces no radiation of wavelengths less than 900 Å. The background should be measured separately for the incident radiation I_o and for each $I(\theta)$ of interest.

The background correction introduces negligible uncertainty in reflectances measured for strong spectral lines. However, errors as large as 2% or 3% could be expected in reflectances measured with very weak lines.

V. DETERMINATION OF THE POLARIZATION OF THE INCIDENT LIGHT

The grating is known to polarize the incident light. Therefore, it is necessary to determine the polarization of the light incident on the sample for a proper evaluation of the optical constants of the cesium film.

The polarization introduced by the 1500 Å blaze grating was measured using a 70°-50°-70° triple reflection polarizer (gold coated). Detailed theory and applications of this polarizer have been discussed by Hamm et al. (1965) and Horton et al. (1969). The polarizer was attached to the exit arm of the monochromator and aligned so that the emerging beam was not deflected as the mirrors were rotated. A photomultiplier tube coated with sodium salicylate was connected to the exit side of the polarizer.

The polarization P of the light emerging from the monochromator was determined by the relation

$$P = \frac{I_p - \rho I_s}{I_s - \rho I_p} \tag{60}$$

where I_p and I_s are the intensities of light transmitted by the polarizer for the plane of incidence of the polarizer parallel and perpendicular, respectively, to the plane of the grating, and ρ is the polarization introduced by the polarizer. The light incident on the grating was assumed unpolarized in this derivation.

Since ρ had been measured earlier, we measured only I_p and I_s in order to obtain P. Figure 7 shows the degree of polarization of the grating used in this experiment.

It is known that the polarization of the grating changes with time. This aging effect is attributed to oxidation and oil contamination of the metallic surface of the grating [Cowan (1969)].

ORNL DWG. 69-14456

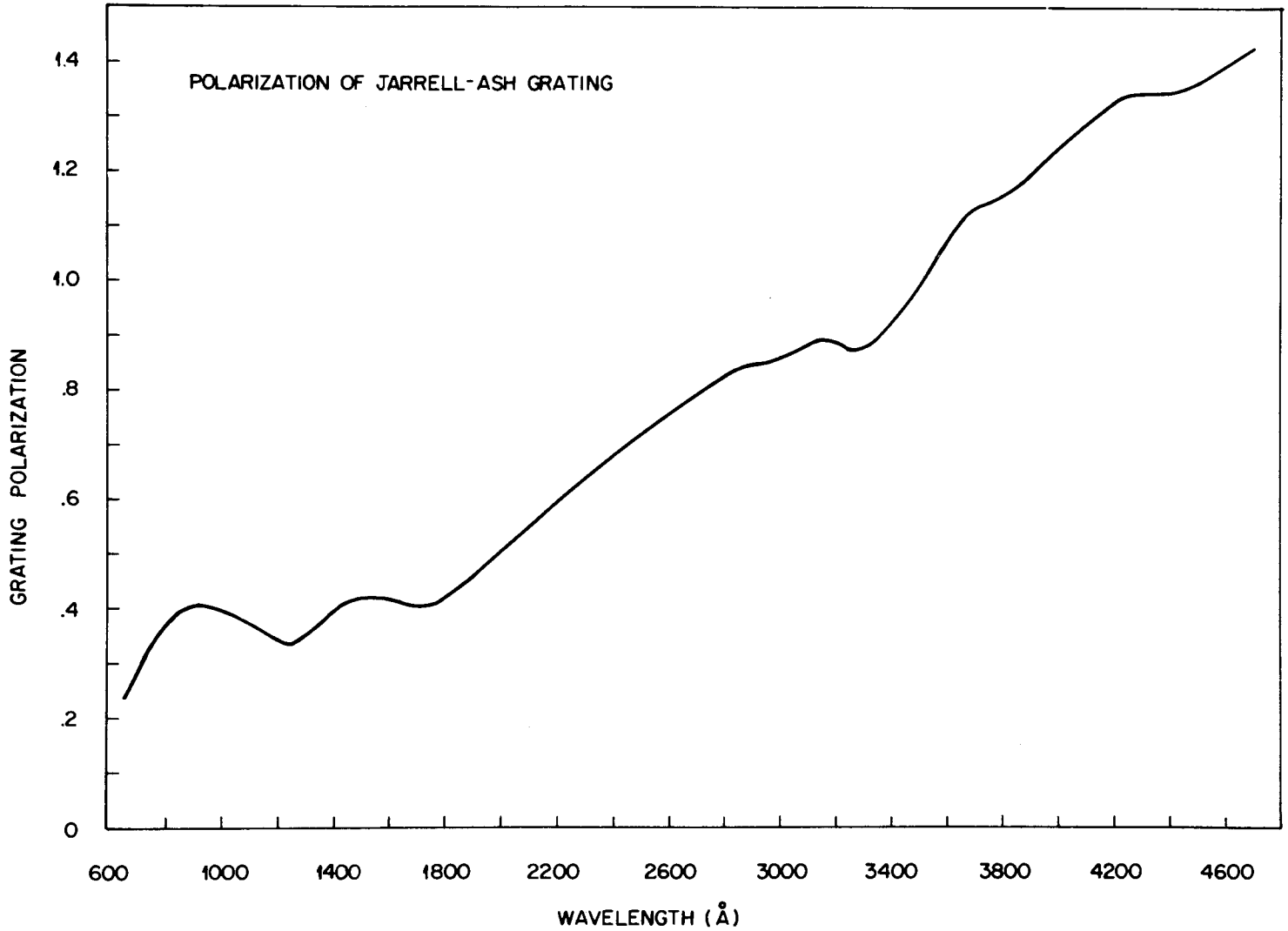

Figure 7. Polarization of 1500 Å blaze grating as a function of wavelength.

CHAPTER VI

DETERMINATION OF OPTICAL CONSTANTS

There are two main methods for the determination of the optical constants of metals: the intensity or photometric method, and the polarimetric method [Beattie (1955), Beattie and Conn (1955), Mayer and Böhme (1964)]. The latter obtains optical constants from measurements of the state of polarization of the light reflected from a surface.

The photometric method requires only the measurement of light intensities. In some cases, the measurement of normal incidence reflection combined with a Kramers-Kronig analysis [Jahoda (1957), Stern (1963)] is sufficient to determine ϵ_1 and ϵ_2. A more general method is to measure the reflection as a function of angle and obtain the optical constants by fitting Fresnel's equations. In a variation of this method, n is determined by finding the angular position of the critical angle for total internal reflection. k is then determined from the slope of the reflectance curve near the critical angle. The "critical angle method" of determining n and k was used in this study.

The critical angle method was used to determine the index of refraction of cesium in the region where the relative index of refraction of cesium is smaller than unity and the absorption coefficient is very small. For a light beam passing from a more dense to a less dense transparent

material, the slope of reflectance as a function of angle of incidence is discontinuous at the critical angle θ_c, which marks the onset of total internal reflection for all angles larger than θ_c. When the extinction coefficient k is zero, the index of refraction of cesium relative to substrate, n_{rel}, is given by

$$n_{rel} = \sin \theta_c . \tag{61}$$

The behavior of the reflectivity near the critical angle is shown in Figure 8 for $n_{rel} = .7$ and $k_{rel} = 0, .02, .05$, and $.10$.

Absorption (that is, $k > 0$) removes the discontinuity in the reflectance curve. Hunter (1964) has shown that to a good approximation the critical angle is the angle θ_m where the slope of reflectance curve is a maximum if $k_{rel} \lesssim .02$. Accordingly, in this case the relative index of refraction of cesium is given by

$$n_{rel} = \sin \theta_m . \tag{62}$$

Hunter pointed out that for $k_{rel} > .02$, n_{rel} obtained from θ_m must be corrected to account for the shift in the position of maximum slope produced by absorption. These shifts are shown in Figure 8 for $k_{rel} = .05$ for which $\sin \theta_m = .718$, and $k_{rel} = .10$ for which $\sin \theta_m = .759$. Failure to correct for this absorption would cause errors of 2.5% and 8% in calculated values of n_{rel}. He also observed that there are other effects that shifted the position of the maximum slope away from the critical angle. Among these are the presence of an absorbing layer, such as oxide, interference

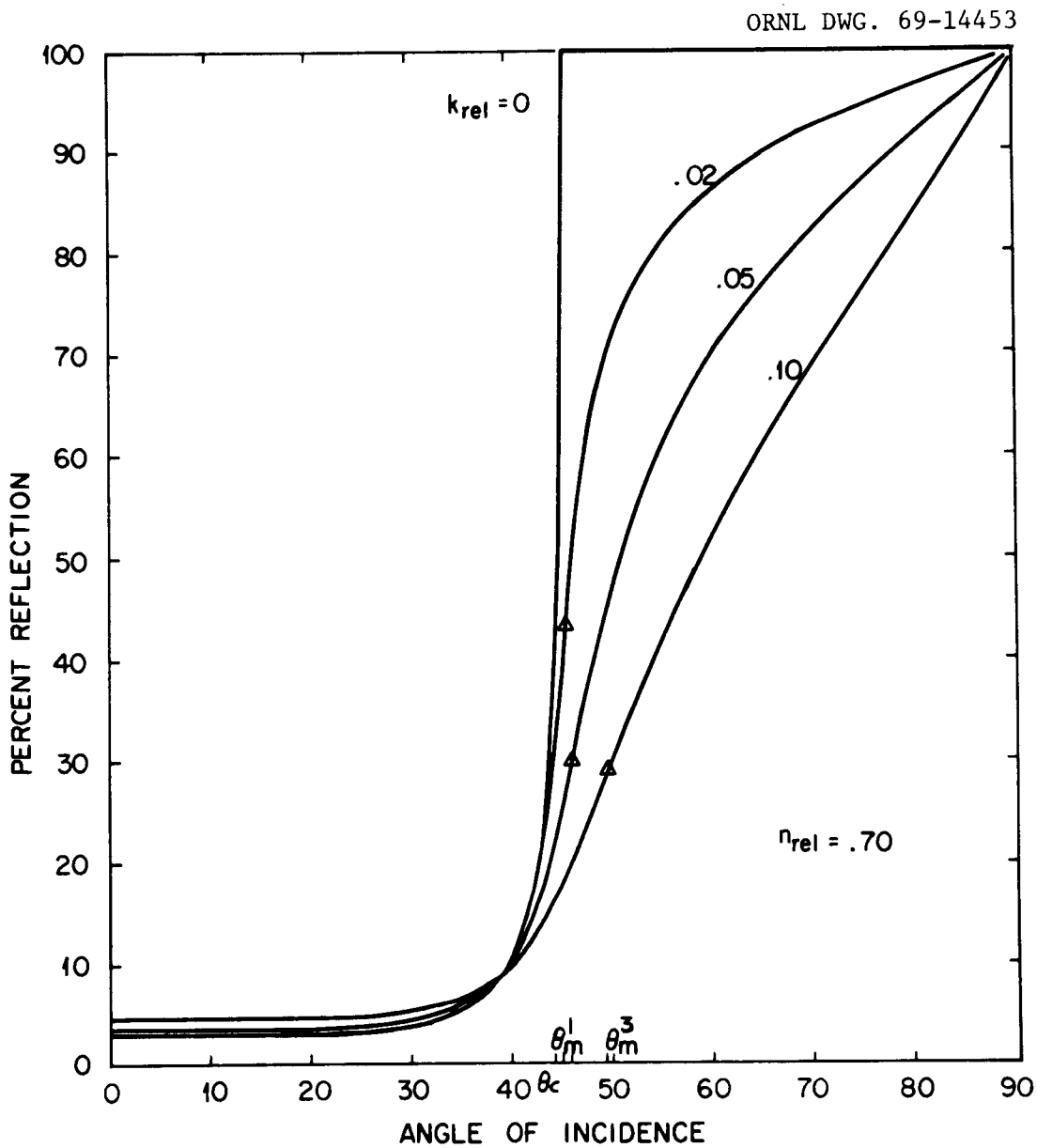

Figure 8. Calculated reflectance versus angle of incidence for $n_{rel} = .7$, $\theta_c = 44° 26'$, and different values of k_{rel}.

Triangles are the positions of θ_m's. The values are $\theta_m = 45° 0'$ for k = .02, $\theta_m^2 = 45° 54'$ for k = .05, and $\theta_m^3 = 49° 26'$ for k = .10.

effects that might be present if the sample is in the form of a layer on a substrate, and polarization of incident radiation. However, these effects could be neglected or minimized if the films were thick (greater than 2000 Å), provided that n_{rel} was measured from θ_m. It is important to note that the accuracy of the determination of n_{rel} depends only on the accuracy of locating θ_m and not on proper normalization of the reflectance curves.

The absolute index of refraction of cesium is given by

$$n = n_s \sin \theta_m \tag{63}$$

where n_s is the index of refraction of the semicylinder. The values of n_s for CaF_2 are shown in Figure 9.

The absorption coefficient may be obtained from the slope of the reflectance curves at the critical angle. Figure 8 shows that the slope is very sensitive to k_{rel}. Figure 10 shows that it does not depend significantly on n_{rel} for a wide range of this variable. This figure shows reflectance curves calculated from Fresnel's equations for $k_{rel} = .03$ and values of n_{rel} ranging from .63 to .89. The maximum slopes of all curves are equal to within 5%.

In practice, the accuracy of the values of k_{rel} calculated from these slopes depends on proper normalization of the reflectance curves. For cesium, the reflectance curves above the critical angle deviate greatly from the ideal theoretical curves. These anomalies are discussed in a later section. Here it is enough to say that we do not have a detailed explanation

ORNL-DWG 69-14446

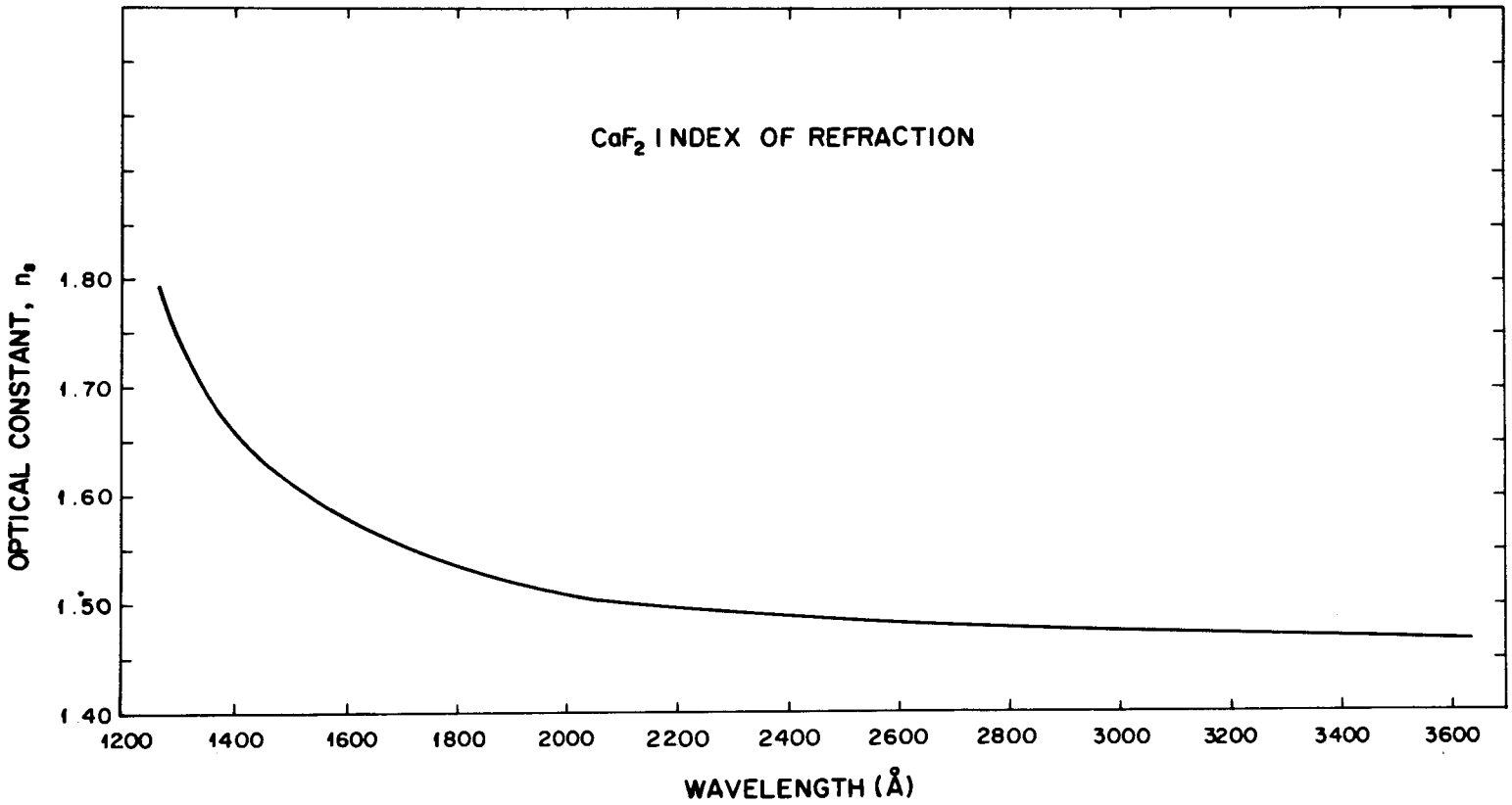

Figure 9. Index of refraction of calcium fluoride as a function of wavelength.

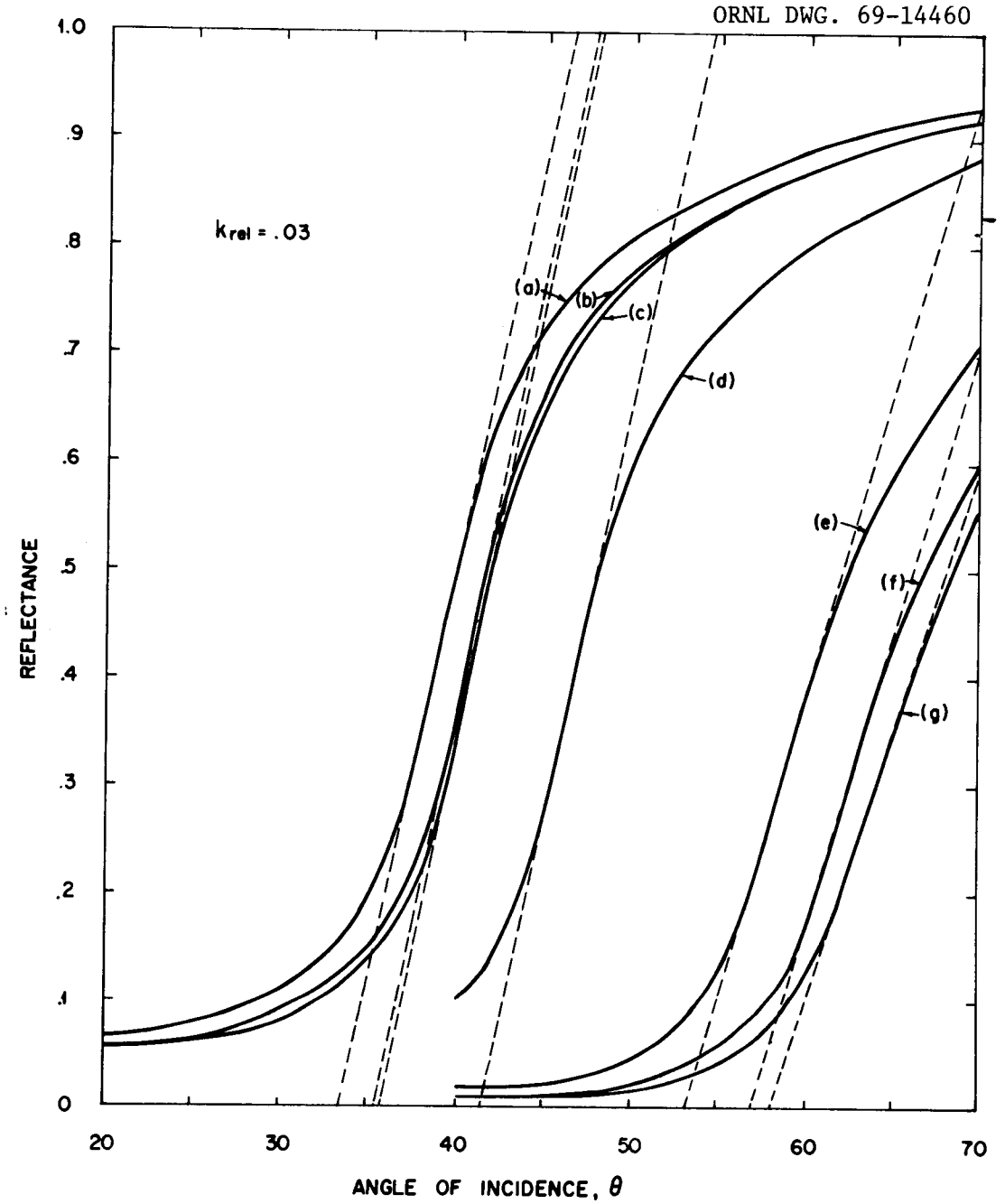

Figure 10. Dependence of the slope of the reflectance at θ_m on n_{rel} and P.

(a) n_{rel} = .63, P = .35
(b) n_{rel} = .65, P = .41
(c) n_{rel} = .65, P = .52
(d) n_{rel} = .72, P = .65
(e) n_{rel} = .85, P = .80
(f) n_{rel} = .88, P = .80
(g) n_{rel} = .89, P = .80

of these anomalies and that, in the absence of such an explanation, the proper normalization of the reflectance curves is not known. The normalization problem introduces uncertainties of about 25% in the quoted values of k_{rel}.

For large k_{rel} values ($k_{rel} > .05$) the effect of polarization of the incident radiation was appreciable in correcting n_{rel} values. The polarization of the grating used as a function of the wavelength is shown in Figure 7, page 43.

The critical-angle technique for determining n_{rel} is advantageous because this technique appears to be free from the serious limitation imposed on the general reflectance method by the formation of the oxide layer at the metal-vacuum side (Figure 11) and because of its relative insensitiveness to surface roughness; the position of θ_m does not vary significantly with roughness, although the magnitude of the slope is reduced. This technique is also useful, especially for small k, for its insensitive dependence of the angle of maximum slope in determining n_{rel}. The error involved in reading θ_m was found to be no more than 2% to 4%.

Figures 11 through 14 show the changes in reflectance of the cesium film due to formation of an oxide layer on the cesium film as time passes following evaporation. The thickness of the oxide layer was not measured. However, several visual cues can be used to indicate the degree of excitation. Cesium metal reflects light above 4400 Å and transmits shorter wavelengths. Consequently, reflected light has a gold tint and transmitted

ORNL DWG. 69-14449

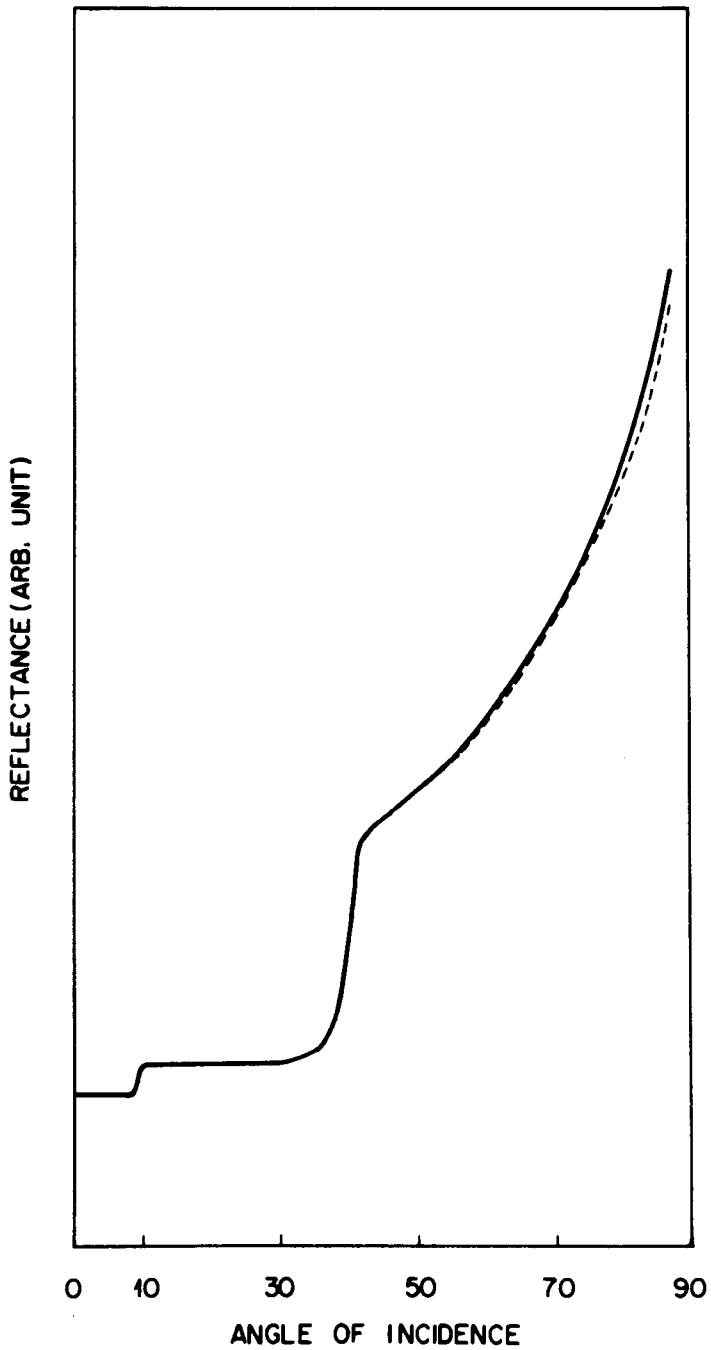

Figure 11. The change in reflectance of the cesium film (thick film) due to formation of an oxide layer for $\lambda = 1295$ Å.

Solid line is for measurement at t = 5 min. after evaporation of the film, and dashed line is for measurement at t = 35 min.

ORNL DWG. 69-14447

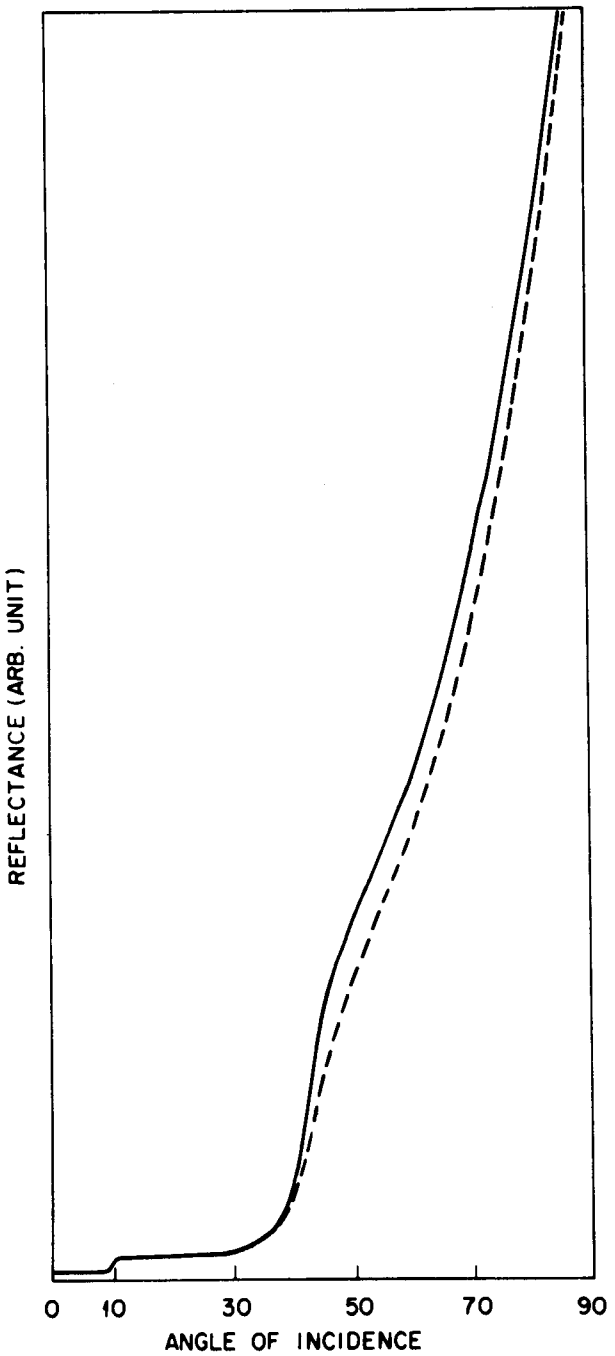

Figure 12. The change in reflectance of the cesium film (thin film) due to formation of an oxide layer for $\lambda = 1536$ Å.

Solid line is for measurement at t = 10 min. after evaporation of the film, and dashed line is for measurement at t = 60 min.

ORNL DWG. 69-14448

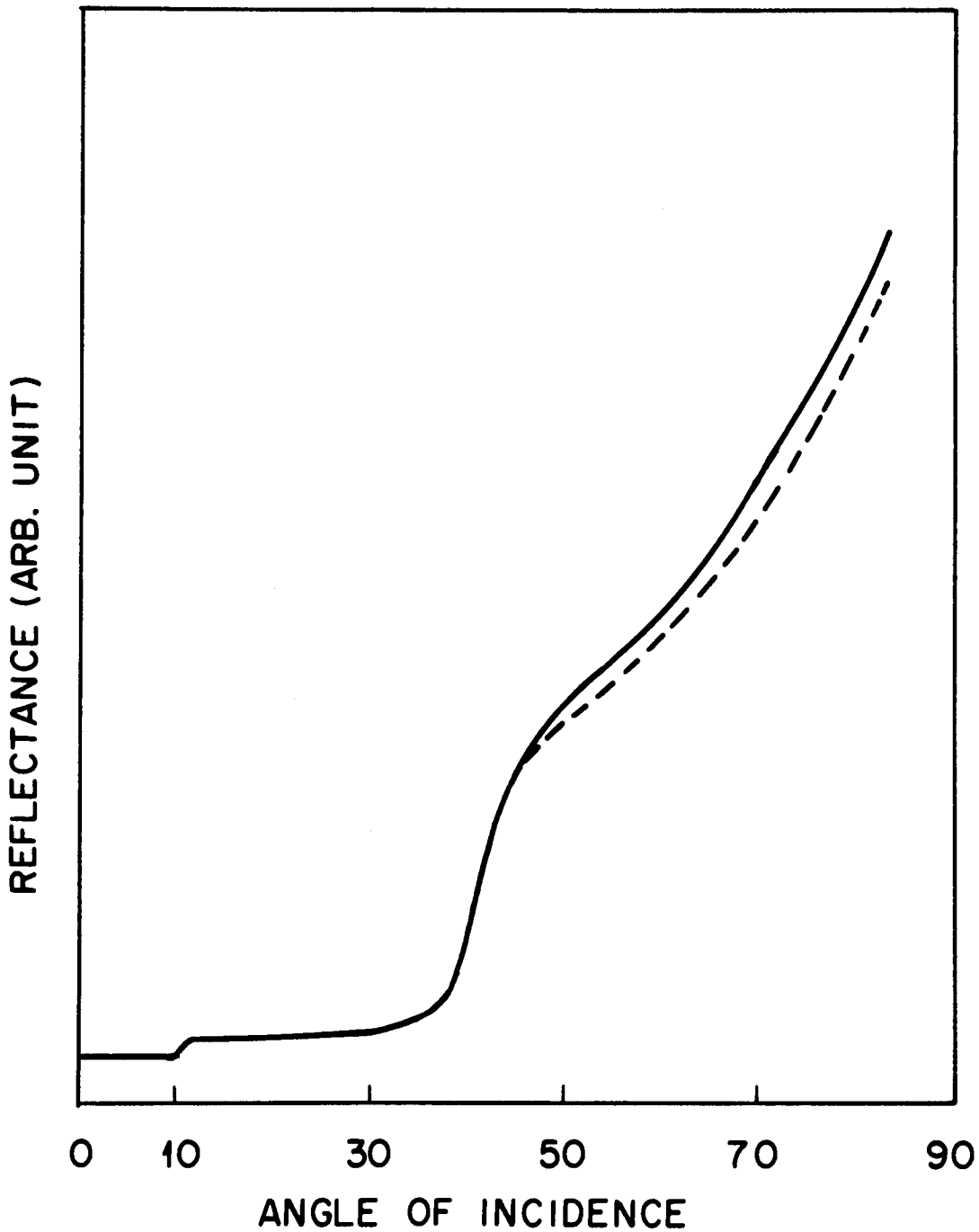

Figure 13. The change in reflectance of the cesium film (thick film) due to formation of an oxide layer for $\lambda = 1477$ Å.

Solid line is for measurement at t = 10 min. after evaporation of the film, and dashed line is for measurement at t = 2 hours.

ORNL-DWG. 69-14445

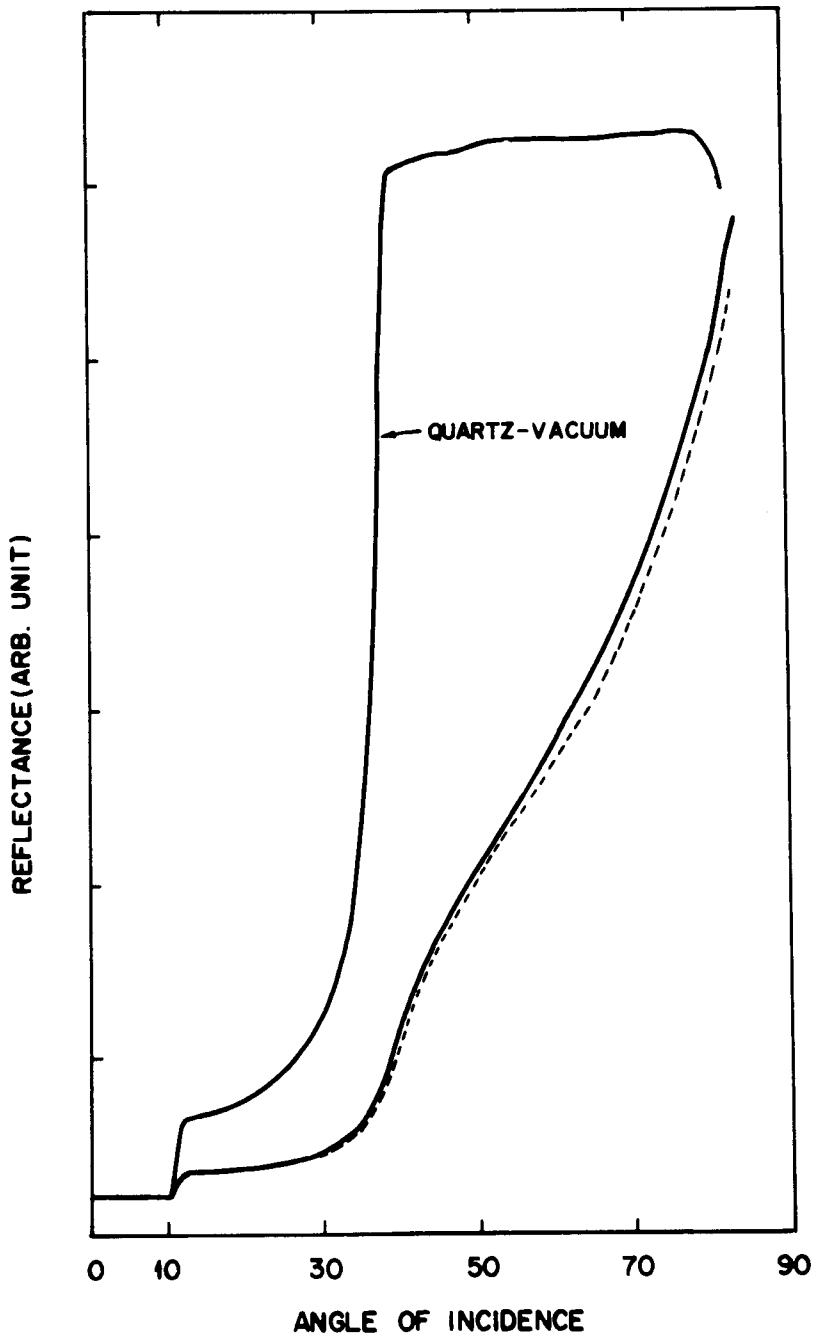

Figure 14. The change in reflectance of the cesium film (thick film) due to formation of an oxide layer for $\lambda = 1761$ Å.

Solid line is for measurement at t = 10 min. after evaporation of the film, and dashed line is for measurement at t = 4 hours.

light is blue. When completely oxidized, the transparency of the film is greatly increased. Immediately after a good evaporation, the film at both the vacuum and the substrate interface has the characteristic gold tint. With time, following evaporation, the vacuum interface of the film becomes increasingly gray. As the oxidation reaches the substrate interface, it is most noticeable in transmission. Small "holes" appear in the film due to the greater transparency of cesium-oxide. These holes then grow until they cover the entire film. At this point the film appears grayish on both surfaces in reflected light.

Since measurements are made at the cesium substrate interface and oxidation proceeds from the opposite face of the film, we would expect little effect on the reflectance curves in the initial stages of oxidation. Reflectances at time t = 5 minutes and at t = 35 minutes for wavelength 1295 Å for a thick film (over 10,000 Å) are shown in Figure 11, page 51. There is no significant change in either θ_m or reflectance $I(\theta)$. In contrast, Figure 12, page 52, shows large deviations in reflectance in both θ_m and $I(\theta)$ for measurements taken at t = 60 minutes at 1536 Å on a thin film. It shows that θ_m is shifted toward larger angle by a half degree for the heavily oxidized film. In Figure 13, page 53, (for λ = 1477 Å, t = 2 hours, and thick film) reflectances in the later measurement are reduced but no change in θ_m is observed. In Figure 14, page 54, (for λ = 1761 Å, t = 4 hours, and thick film) θ_m is shifted by .3° which increased n from 1.006 to 1.012. We may conclude that the effect of the oxide layer is to shift the values of n toward

slightly larger values when measurements are made within an interval of a few hours following evaporation on a thick film.

From a comparison of Figures 8, page 46, and 11 through 14, pages 51 through 54, it is clear that the experimental reflectances do not satisfy the Fresnel relation for angles larger than θ_m. The reflectances above the critical angle are much depressed below those predicted by theory for corresponding angles. This anomalous behavior of the reflectance is not well understood. Two interpretations are possible. The first is that two separate scattering mechanisms are operating. Part of the beam undergoes the expected critical angle reflection at the substrate-metal interface and the remainder is scattered by some other process (for example, diffuse scattering by patches of Cs_2O in the interface). In this case the theoretical curves should be normalized only to that fraction of the total beam undergoing critical angle reflection. In most cases this is only one-third to one-half of the total incident beam. From inspection of Figures 10, page 49, and 11 through 14, it is clear that the reflectance of the remaining light is small below the critical angle and increases to unity at glancing incidence.

This type of interpretation is consistent with the assumption that the anomalies in $I(\theta)$ result from experimental problems in preparing a clear, planar substrate-cesium interface with average roughness of much less than 1000 Å. Additional experiments are planned which will use different substrate cleaning techniques and much better vacuums during evaporation. It should be noted that the procedures used in this work have provided much better reflectance curves for Na, K, and Rb. At the least, the large anomalies in

$R(\theta)$ for cesium demonstrate that it is a technically difficult material with which to work.

The second possibility is to normalize $I(\theta)$ to the total beam incident on the film as measured by the reflection from the substrate-vacuum interface. In most imaginable models this implies that the anomalies are not associated with experimental problems and that all, or nearly all, of the beam is reflected by a "good" interface. The anaomalies then reflect a failure of Fresnel's equation to describe the physical processes occurring during reflection at an interface. Some unknown process must depress the reflectance curves above the critical angle. An example of a possible process not accounted for by these Fresnel equations is the generation of a surface plasmon in the interface. We cannot usefully speculate on such possibilities until it is determined if improved vacuum and cleaning procedures modify the reflectance curves.

The absorption coefficients given in this paper were obtained by assuming that only part of the beam undergoes total internal reflection. For small k ($\lesssim .5$), $I(\theta)$ was normalized to that portion of the beam estimated to have undergone critical-angle reflectance and k was calculated from the slope of $R(\theta)$ at the critical angle. For large k, $R(\theta)$ in the vicinity of the critical angle was fitted to computer generated reflectance curves to obtain n and k, and the portion of the reflectance curve well above the critical angle was ignored.

In practice the reflectance curves were normalized by fitting theoretical curves to the experimental data at $\theta = 20°$ and near the top of the portion of $R(\theta)$ showing critical angle behavior (about 45°). Figure 15 shows curves normalized in this way for wavelengths of 1817 Å and 2260 Å. The curves show $R(\theta)$ for a polarization of .42, n_{rel} of .65 ($\theta_c = 42°\ 32''$) and k_{rel} between .02 and .12. They are normalized to the data at points marked by a rhombus (1817 Å) and a square (2260 Å). The values of k_{rel} determined are .05 and .09, respectively. For a given normalization, the uncertainty in the value of k is no more than 10%. When the uncertainties in the normalization are taken into account, the values of k obtained have an estimated uncertainty of about 20% for $k_{rel} \leq .02$ increasing to about 30% for $k_{rel} \simeq .1$.

The values of n and k obtained in our analysis are listed in Table 1 for four samples. The values of n obtained from all samples are reproduced within a few percent over the whole range of wavelengths considered, while the scatter in the k values is very large. The k values used in the following discussion were obtained by drawing a smooth curve through the averaged values of k. In Table 1, $\langle\ \rangle$ represents the averaged values of n and k, and $\{\ \}$ gives values obtained from the smoothed curve. Figure 16 shows the experimentally determined values of n and k. The solid lines give the averaged smooth curve.

If our data are normalized using the second type of normalization mentioned above, the values of n_{rel} obtained are not significantly changed.

ORNL DWG. 69-14458

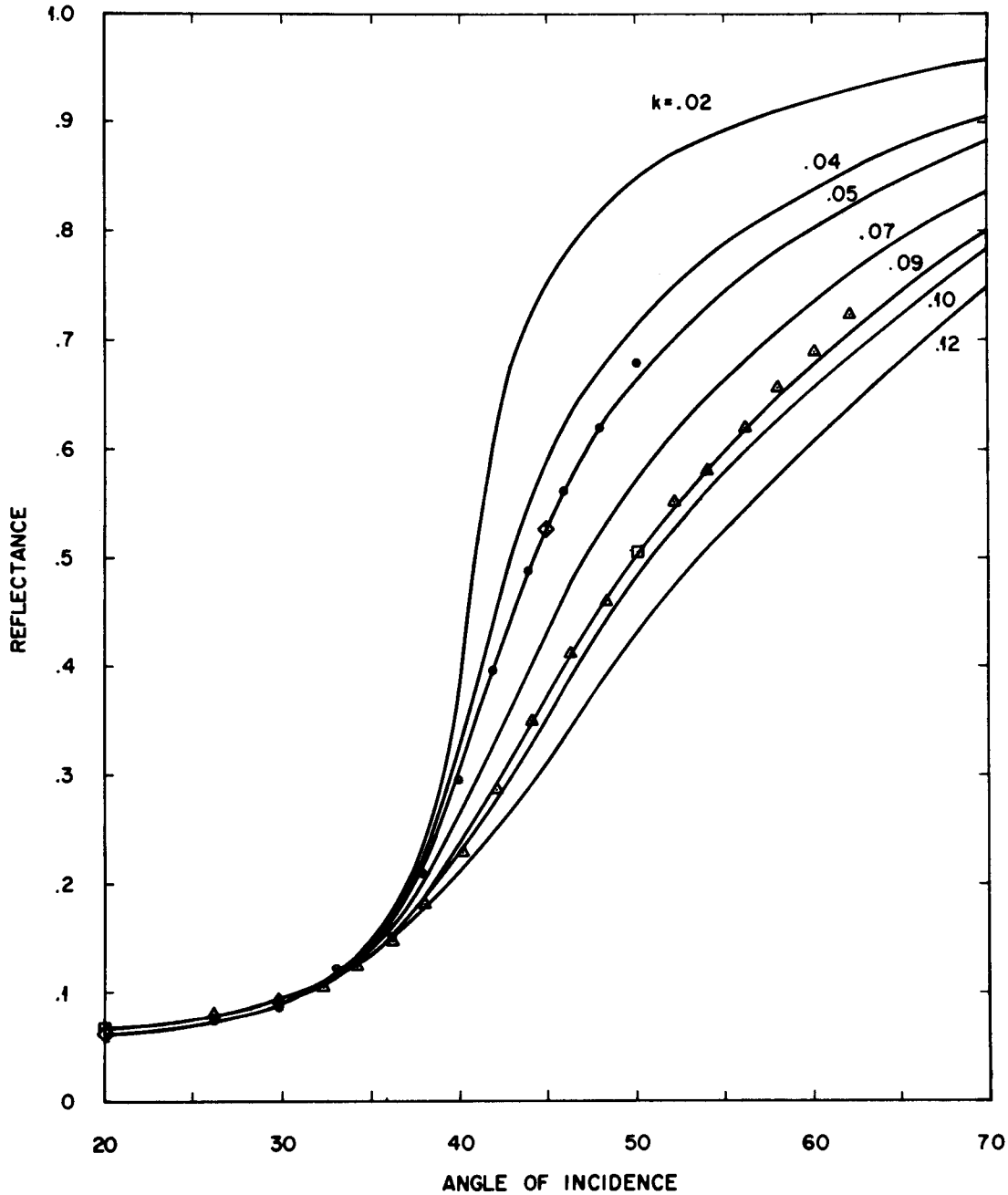

Figure 15. Fitting of experimental reflectance at 1817 Å (O) and 2260 Å (Δ) to theoretical curves.

Data are normalized at $\theta = 20°$ for both, at $\theta = 44°$ (◇) for $\lambda = 1817$ Å, and at $\theta = 48°$ (□) for $\lambda = 2260$ Å.

Table 1. n and k of Cs as a function of wavelength

	n						k					
λ(Å)	Film A	Film B	Film C	Film D	⟨n⟩	{n}	Film A	Film B	Film C	Film D	⟨k⟩	{k}
1294	1.096				1.096	1.109	.021				.021	.023
1372	1.090	1.079	1.082	1.109	1.090	1.090	.025	.025	.027	.033	.027	.028
1418	1.084	1.092	1.081	1.083	1.085	1.080	.033	.033	.033	.033	.033	.030
1477	1.065	1.078	1.067	1.058	1.067	1.067	.032	.040	.032	.032	.034	.033
1536	1.060	1.059	1.061	1.051	1.058	1.054	.040	.032	.032	.032	.034	.036
1597	1.040	1.050			1.045	1.040	.047	.047			.047	.040
1625	1.039	1.041	1.034	1.031	1.036	1.032	.047	.047	.031	.039	.041	.042
1687	1.034	1.015	1.023	1.022	1.023	1.022	.054	.078	.047	.047	.056	.048
1750	1.013	1.012		1.004	1.009	1.010	.077	.077		.046	.066	.057
1817	1.001	1.007	1.007	.999	1.003	1.002	.062	.108	.062	.062	.073	.064
1862	.995				.995	.994	.076				.076	.071
1897	.986	.992	.986	.978	.985	.988	.076	.091	.061	.047	.069	.076
1963	.982	.986	.988	.986	.985	.981	.106	.121	.091	.091	.102	.086
2036	.986	.981		.974	.980	.976	.091	.121		.106	.106	.095
2115	.963	.978		.966	.969	.970	.090	.090		.135	.105	.105
2166	.963	.963	.947	.957	.957	.965	.150	.090	.149	.127	.129	.112
2260	.955			.950	.952	.954	.119			.134	.126	.125
2282	.952	.958		.948	.952	.952	.119	.179		.120	.139	.128
2377	.953			.947	.950	.948	.134			.149	.141	.140

ORNL DWG. 69-14450

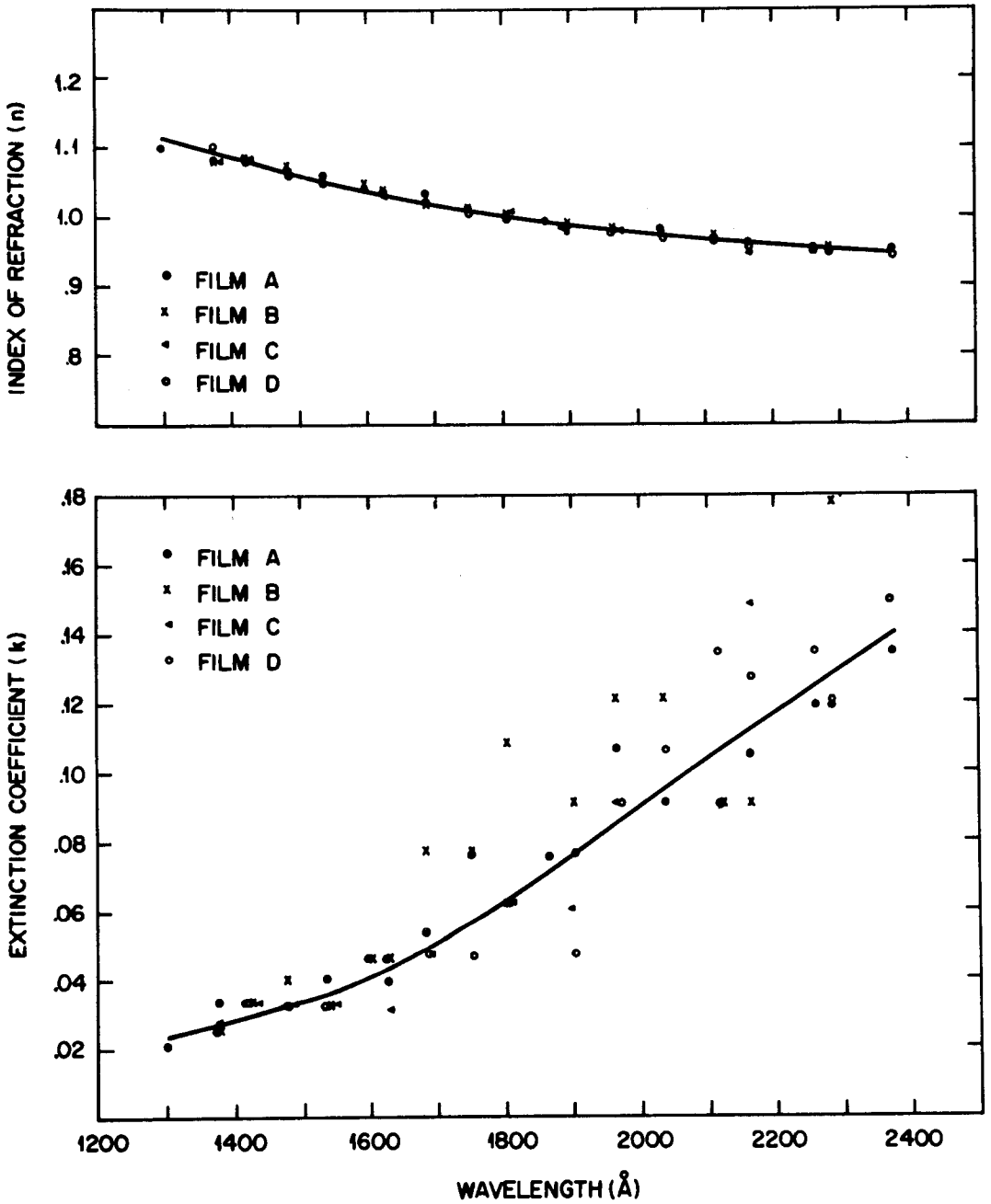

Figure 16. Experimentally determined n and k for cesium.

However, all values of k are increased by roughly a factor of two. This normalization was not used in interpreting the data for several reasons. First, we were not able to imagine a physical process that would produce such large deviations from Fresnel's equations. Second, the values of k obtained in this way were not internally consistent; for example, using these values of k, the measured normal reflectances, given by Equation (29) were too small to agree with experiment. And, finally, the results obtained in this way were much too large to be consistent with those obtained by other workers. The results of various workers are discussed in the following chapter.

CHAPTER VII

DISCUSSION OF RESULTS

Values of the real and imaginary parts of the dielectric constant may be derived from the experimentally determined n and k from the relations

$$\epsilon_1 = n^2 - k^2$$

and

$$\epsilon_2 = 2nk.$$

Our values of ϵ_1 are plotted as a function of λ^2 in Figure 17. Also plotted are data obtained at longer wavelengths by Ives and Briggs (1937b). In this work the values of ϵ_1 obtained are virtually unaffected by the uncertainties in k since for $n \simeq 1$ and $k \lesssim .1$, $k^2 \lesssim .01\, n^2$. ϵ_1 may be fitted to the theoretical expression given by Equation (48).

Prior to further discussion we want to differentiate between "plasma frequencies" ω_b and ω_p. In Equation (48) Cohen (1958) defines a plasma frequency ω_p where $\epsilon_1 = 0$, while ω_b may be measured from the slope of the curve, ϵ_1 versus λ^2. The two are the same only when $4\pi n_o \alpha_1 = 0$. However, both are often referred to as the plasma frequency [for example, ω_p is called plasma frequency by Cohen (1958) and Pines (1963), while ω_b is called plasma frequency by Mayer and Hietel (1966)]. We will call ω_p the "effective plasma frequency" or "plasma frequency," and ω_b the "optical plasma frequency." From Equations (49) and (28) the ratio of ω_o^2 to ω_b^2

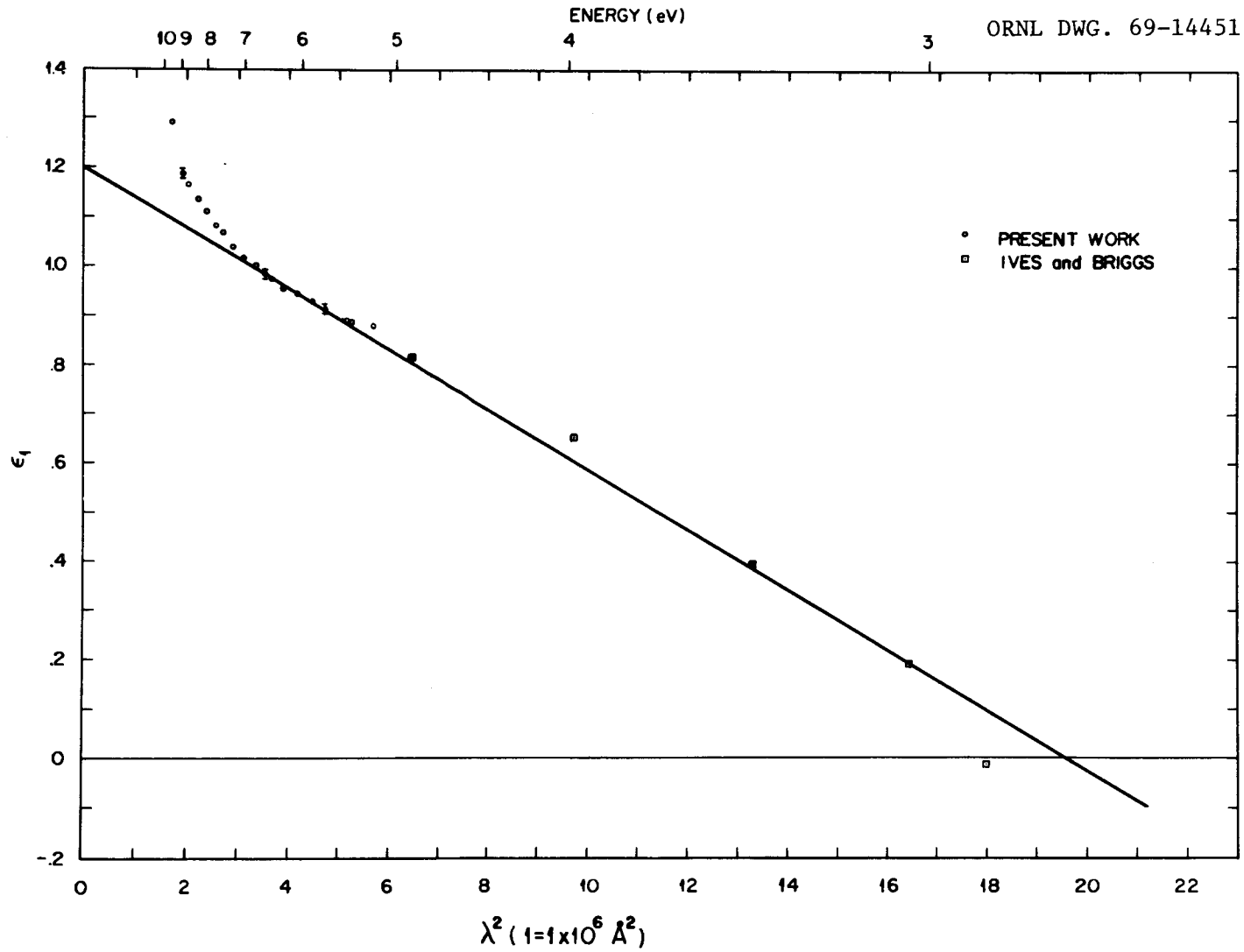

Figure 17. Real part of the complex dielectric constant versus square of photon energy.

gives directly the ratio of m_{opt} to m:

$$\frac{\omega_o^2}{\omega_b^2} = \frac{m_{opt}}{m}$$

where ω_o is calculated plasma frequency of a free electron (3.45 eV or 3600 Å for cesium).

The points between the scale units of 3.0 and 5.4 in λ^2 are close to straight line connecting Ives and Briggs' (1937b) data points. This straight line is predicted by Equation (48) or (25). The last two circles lie above this straight line. This shift may be due to the presence of an oxide layer since the presence of such a layer tends to shift the values of n toward larger values.

A striking feature in this work is the deviation of data points from the straight line for wavelengths below 1732 Å (7.16 eV). As discussed in the theory, increases in ϵ_1 with increasing frequency may be associated with strong interband transitions lying at higher frequencies. We suspect that the strong transition is the excitation of $(5p)^6$ core electrons. We estimate from calculations of atomic energy levels by Bearden and Burr (1965) that this excitation has a threshold energy of about 11.4 eV (1089 Å). Formally, the shift in ϵ_1 may be accounted for through the third term in Equation (46) by replacing the band index c by s designating a core state, and the unoccupied band index i by c′, which designates the unoccupied portion of the conduction band. It is true, of course, that the core polarization and other

interband transitions affect ϵ_1 in this region. It seems probable, however, that these are fully accounted for by the term $4\pi n_o \alpha_1$ and thus would not result in deviation from Equation (46).

The parameters α_1, ω_b, and ω_p may be obtained from Figure 17, page 64. The value of $1 + 4\pi n_o \alpha_1$ is given by the point of intersection of the straight line with the ordinate:

$$1 + 4\pi n_o \alpha_1 = 1.20 \pm .03$$

where $n_o = n_c$ since cesium is monovalent. The value of λ_b is given by the slope of the straight line:

$$\lambda_b = \left(\frac{\pi c^2}{me^2} m_{opt}\right)^{\frac{1}{2}} = 4031 \pm 50 \text{ Å} ,$$

or

$$\hbar\omega_b = 3.08 \pm .01 \text{ eV}$$

from which one finds the optical effective mass

$$\frac{m_{opt}}{m} = 1.25 \pm .03$$

where m is the rest mass of a free electron. The plasma wavelength λ_p is determined by the extrapolation of the line through the data points to $\epsilon_1 = 0$:

$$\lambda_p = 4354 \pm 55 \text{ Å}$$

or

$$\hbar\omega_p = 2.85 \pm .01 \text{ eV} .$$

Table 2 gives the dielectric constants of cesium obtained in this and other experiments.

Table 2. Polarizability, effective masses, and the plasma energy of cesium

Investigator	$4\pi n_o \alpha_1$	$4\pi n_o \alpha_o$	m_{opt}/m	$\hbar\omega_b$	$\hbar\omega_p$	Method
Present work	$.20 \pm .03$		$1.25 \pm .03$	3.08	2.85	Critical angle
Cohen's analysis of Ives and Briggs' data [Cohen (1958)]	$.37 \pm .03$		$1.02 \pm .02$	3.34[a]	2.91	Ellipsometry
Mayer and Hietel (1966)	$.17 \pm .01$		$1.45 \pm .02$	2.86	2.65[b] 2.86[c]	Ellipsometry
Tessman *et al.* (1953) (from Cohen's analysis)		.38				Polarizability of Cs ions and Cs halide of crystal
Lander and Morrison (1969)					2.9	Energy loss
Hartley (1967)					$2.94 \pm .004$	Energy loss
Wood (1933a)					2.82	Ellipsometry

[a] Calculated from Cohen's analysis.

[b] Calculated from $\hbar\omega_p = \hbar\omega_b \Big/ \sqrt{1 + 4\pi n_o \alpha_1}$.

[c] Evaluated from energy loss function.

In principle, α_1 exceeds α_o by the value of the conduction electron polarizability which at these frequencies should be relatively small. However, in the present work α_1 is considerably smaller than α_o given by Tessman et al. (1953) who measured the polarizability of cesium ions in cesium halide crystals.

The values of ω_b and ω_p listed in Table 2 are derived from our data combined with those of Ives and Briggs (1957b). ω_p, obtained from the x intercept, is essentially unchanged in our analysis since it is determined primarily by the data of Ives and Briggs. The values of $4\pi n_o \alpha_1$ and ω_b and the derived quantity m_{opt}/m are significantly different from those of Ives and Briggs because our data define more accurately the slope of the curve of ϵ_1 versus λ^2 and the y intercept.

The optical absorption of cesium is shown in Figure 18 where the optical conductivity $\sigma = \epsilon_2 \omega / 4\pi$ is plotted versus $\hbar\omega$. The circles are our data, the triangles are those of Mayer and Hietel, and the rectangles are those of Ives and Briggs. The large error bars reflect the large scatter in measured values of k.

Since our data cover a limited energy range, we have combined our results with those of Mayer and Hietel and those of Ives and Briggs at lower energies. The most interesting feature of the combined data is a broad peak between 3.5 and 7.5 eV, with a smoothly falling curve above 7.5 eV. The peak maximum occurs at approximately the junction between our results and those of Mayer and Hietel and Ives and Briggs.

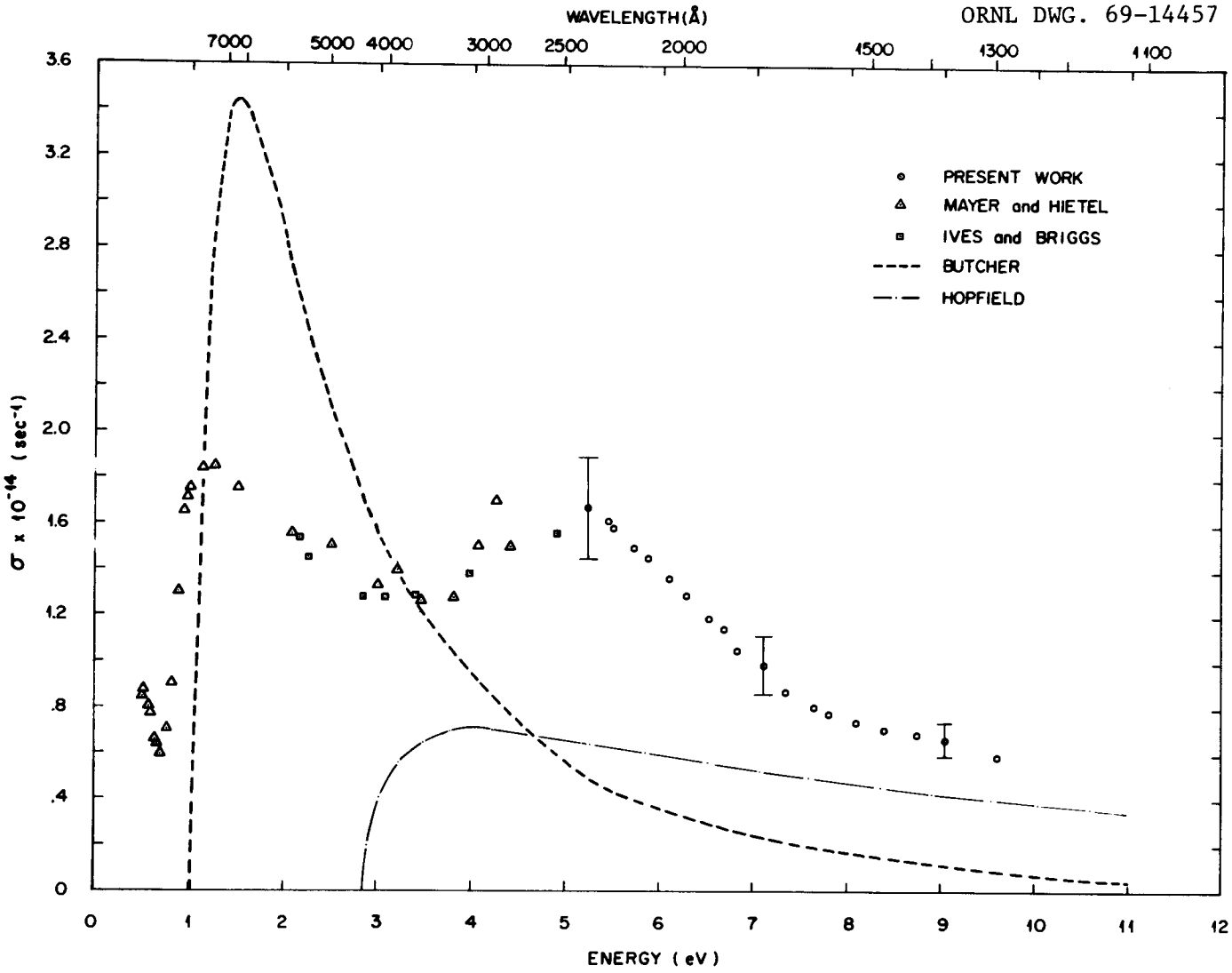

Figure 18. Optical conductivity versus photon energy ($\hbar\omega$).

We believe that the evidence of the combined data is sufficiently strong to confirm the existence of the peak, but it is clearly not accurate enough to define its shape or to give the exact position of the maximum. There seems to be no reason to doubt the generally rising conductivity observed by Mayer and Hietel (1966) and Ives and Briggs (1937b) between 3.5 and 4.5 eV or the generally falling conductivity we observe above 5 eV. Shifting our results within error bars shifts the apparent position of the peak maximum from 4.5 to 5.0 eV, but does not eliminate it. We note that use of the alternative extreme of normalization discussed in the previous chapter results in an increase of k and thus of σ by approximately a factor of two. Such values would clearly be difficult to reconcile with the data taken at lower photon energies. In a sense, the analysis we use in interpreting the critical angle data gives the minimum values of k and σ consistent with our data. With these values, the peak centered at $4.5 \pm .5$ eV is a consistent and well-defined feature of the experimentally measured conductivity.

The peak is not explained by any of the absorption mechanism for which detailed calculations have been made for the alkali metals. The Drude free-electron absorption is effective at much lower frequencies and can account for only a few percent of the absorption observed above 4 eV. Butcher (1951) has calculated interband absorption using a nearly-free-electron model for transitions from the conduction band to higher lying bands.

Butcher's (1951) approximation for the intrinsic absorbing power of a homogeneous isotropic medium due to photoexcitation is given by

$$\sigma_{photo}(\omega) = \frac{4\sqrt{2}\, m a e^2 \pi^2}{h^4} \left| V_{\sqrt{2}} \right|^2 \frac{(\omega - \omega_o)(\omega_1 - \omega)}{\omega^3} \tag{64}$$

with

$$\omega_o = \left(\frac{\sqrt{2}\, h}{ma^2}\right)(\sqrt{2}\,\pi - a k_m), \text{ and } \omega_1 = \left(\frac{\sqrt{2}\, h}{ma^2}\right)(\sqrt{2}\,\pi + a k_m).$$

Here a is the lattice constant and has the value of 6.05 Å for cesium, $k_m = \frac{\sqrt[3]{6\pi^2}}{a}$, radius of the Fermi surface, and $|V_{\sqrt{2}}|$ is the magnitude of the Fourier component in the (1, 1, 0) direction (of $\vec{k}$ vector within a first Brillouin zone) of the self-consistent field of a b.c.c. lattice; $2|V_{\sqrt{2}}|$ is the energy gap across the surface of the first Brillouin zone according to the nearly-free-electron approximation, and its value is 1.044 eV for cesium; -e and m are, respectively, the charge and mass of a free electron, and h is the Planck constant. $\nu_o = \omega_o/2\pi$ is known as the absorption limit and has the value of 2.37×10^{14} sec^{-1} for cesium. The result of this calculation is shown in Figure 18, page 69, as a dashed line.

The peak in Mayer and Hietel's (1966) data between 1 and 2 eV is adequately explained by Butcher's calculation. Other authors [Animalu (1967), Meessen (1961), Ron and Tzoar (1963)] have refined Butcher's calculation to obtain better quantitative agreement with the low energy peak, but none of the existing calculations give an absorption peak at higher energies.

Butcher's (1951) calculations were directed primarily towards accounting for the absorption in alkali metals of lower atomic number than cesium. They were made for a single free electron outside an ion core, with no explicit account taken of energy bands formed from d and f states with the principal quantum number of core electrons. In particular, for cesium absorption by transitions to bands formed from the 5s, 5p, and higher, $n = 5$ orbitals is approximately calculated, but transitions to bands formed from 4d and 4f states are not considered. The "d bands" form a prominent feature of the cesium band structure at energies 2 to 3 eV above the Fermi level and the "f bands" at energies 5 to 6 eV above the Fermi level (see Figure 3, page 20). Transitions to these bands may account for the anomalous absorption peak. If such is the case the calculated band structures are in error by the order of 1 eV since there are no large concentrations of final states at the observed energies. A calculation of the absorption due to these transitions has not been made. In addition to the mismatch in energy with calculated values 4 to 5 eV above the Fermi level, we believe that the oscillator strengths for such transitions are too small to account for the observed absorption peak.

A second possible explanation of the peak is that it represents absorption associated with the excitation of collective modes (plasmons). The oldest and perhaps most soundly-based calculation is that of Hopfield (1965). Collective effects enter through a change in the effectiveness of electronic shielding at energies above the plasma energy, $\hbar\omega_p$. Ritchie (1969)

has shown that the frequency dependence of the Hopfield contribution to σ for frequencies just above ω_p is

$$\frac{\omega_p^3}{\omega^2}\left(\frac{\omega^2}{\omega_p^2} - 1\right)^{\frac{1}{2}} .$$

This frequency dependence is plotted with an arbitrary vertical scale as a dash-dot curve in Figure 18, page 69. $\hbar\omega_p$ is taken as 2.85 eV. Neglected factors will cause the high energy tail to be depressed below the value given by the above expression with the result that the peak will be sharper and have a maximum at a slightly lower energy than that given by this expression. We see that the experimental peak occurs at too high an energy to be adequately explained by Hopfield's (1965) mechanism.

Other absorption mechanisms associated with plasmon-assisted transitions have been suggested by Lundgvist and Lydén (1969). It seems highly probable that the eventual explanation of the absorption peak will involve the excitation of collective modes.

A peak in σ comparable with the high energy peak for cesium has not been found for the other alkali metals. Na and perhaps K show a much smaller peak [Sutherland (1969)]. We should ask if there is any independent evidence indicating that plasmon effects are more important for absorption in cesium than in these other similar materials. Some evidence is available that they are. The most general argument depends on the fact that a photon cannot excite a single plasmon directly and conserve momentum in the

interaction. Some third particle must conserve momentum. A measure of the strength of the coupling of the plasmon mode to single electron states is given by the width of the plasmon excitation peak in $\mathrm{Im}(1/\tilde{\epsilon})$, the energy loss function for fast electrons. The peak is much broader in cesium than in the other alkalies.

Similar conclusions may be drawn from the photoemission data of Smith and Spicer (1969) who find that effects associated with collective effects are stronger in cesium than in the other alkalies. On the basis of similar photoemission measurements on cesium alone, Callcott (1969) suggested that the energy losses observed in photoemission accompany the absorption of the photon rather than during subsequent transport to the surface. A theoretical proposal to account for the photoemission effects was made by Sutton (1969).

In view of the possible importance of the anomalous peak to testing theories of absorption by collective modes, further experiments are planned that should give more accurate values of k, $\tilde{\epsilon}$, and σ over a range of energies spanning the absorption peak. The measurements reported here will be repeated under better vacuum conditions and reflectance measurements at a cesium-vacuum interface are planned.

These purely optical studies will be supplemented by photoemission studies and perhaps by studies of diffuse reflectances.

BIBLIOGRAPHY

BIBLIOGRAPHY

Animalu, A. O. E., Phys. Rev. 163, 557, 562 (1967).

Appelbaum, J. A., Phys. Rev. 144, 435 (1966).

Bearden, J. A., and A. F. Burr, Atomic Energy Level (U.S.A.E.C., Division of Technical Information Extension, Oak Ridge, Tennessee, 1965).

Beattie, J. R., Phil. Mag. 46, 235 (1955).

Beattie, J. R., and G. R. T. Conn, Phil. Mag. 46, 223 (1955).

Born, M., and E. Wolf, Principles of Optics (3rd ed., Pergamon Press, London, 1965).

Butcher, P. N., Proc. Phys. Soc. (London) 64A, 765 (1951).

Callaway, J., and E. L. Haase, Phys. Rev. 108, 217 (1957).

Callcott, T. A., and A. U. MacRae, Phys. Rev. 178, 966 (1969).

Cohen, M. H., Phil. Mag. 3, 762 (1958).

Cohen, M. H., Phys. Rev. Letters 12, 664 (1964).

Cohen, M. H., "Interpretation of the Optical Properties of the Alkali Metals," in Optical Properties and Electronic Structure of Metals and Alloys, ed. F. Abeles (North Holland Publishing Co., Amsterdam, 1966).

Cohen, M. H., and J. C. Phillips, Phys. Rev. Letters 12, 662 (1964).

Cowan, J. J., E. T. Arakawa, and L. R. Painter, Applied Optics 8, 1734 (1969).

Drude, P., Ann. Physik 1, 566 (1900).

Drude, P., Ann. Physik. 14, 936 (1904).

Ferrell, R. A., "Optical Properties of the Alkali Metals," in Optical Properties and Electronic Structure of Metals and Alloys, ed. F. Abeles (North Holland Publishing Co., Amsterdam, 1966).

Fröhlich, H., Z. Phys. 81, 297 (1933).

Fröhlich, H., Electronen Theorie der Metalle (Julius Springer Verlag, Berlin, 1936).

Fujioka, V., Z. Phys. 76, 537 (1932).

Ham, F. S., Phys. Rev. 128, 82, 2524 (1962).

Hamm, R. N., R. A. MacRae, and E. T. Arakawa, J. Opt. Soc. Am. 55, 1460 (1965).

Hartley, B. M., Phys. Letters 24A, 396 (1967).

Hayes, J. D., M.S. Thesis, Vanderbilt University (1968).

Hopfield, J. J., Phys. Rev. 139A, 419 (1965).

Horton, V. G., E. T. Arakawa, R. N. Hamm, and M. W. Williams, Appl. Optics 8, 1734 (1969).

Hunter, W. R., J. Opt. Soc. Am. 54, 15 (1964).

Ives, H. E., and H. B. Briggs, J. Opt. Soc. Am. 27, 181 (1937a).

Ives, H. E., and H. B. Briggs, J. Opt. Soc. Am. 27, 395 (1937b).

Jahoda, F. C., Phys. Rev. 107, 1261 (1957).

Kenney, J. F., Quarterly Progress Report, Solid State and Molecular Theory Group, M.I.T., 66, 3 (1967).

Kronig, R. deL., Proc. Roy. Soc. (London) 124, 409 (1929).

Kronig, R. deL., Proc. Roy. Soc. (London) 133, 225 (1931).

Kronig, R. deL., Nature 132, 601 (1933).

Kronig, R. deL., Nature 133, 211 (1934).

Lander, J. J., and J. Morrison, Surface Science 14, 465 (1969).

Lorentz, H. A., Theory of Electrons and its Applications to the Phenomena of Light and Radiant Heat (G. E. Stechert and Co., New York, 1909).

Lundqvist, B. I., and C. Lydén, to be published (1969).

Mahanti, S. D., and T. P. Das, Phys. Rev. 183, 674 (1969).

Mayer, H., and H. Böhme, J. Phys. 25, 81 (1964).

Mayer, H., and B. Hietel, "Experimental Results on the Optical Properties of the Alkali Metals," in Optical Properties and Electronic Structure of Metals and Alloys, ed. F. Abeles (North-Holland Publishing Co., Amsterdam, 1966).

Meessen, A., J. Phys. Radium 22, 135 (1961).

Mott, N. F., and H. Jones, The Theory of the Properties of Metals and Alloys (The Clarendon Press, Oxford, 1936).

Nathanson, J. B., Phys. Rev. 25, 75 (1925).

Nettel, S. J., Phys. Rev. 150, 421 (1966).

Overhauser, A. W., Phys. Rev. Letters 13, 190 (1964).

Painter, L. R., M.S. Thesis, University of Tennessee (1968).

Payan, R., and D. Roux, Acad. Sc. Paris, C.R. 267B, 1173 (1968).

Pines, D., Elementary Excitation in Solids (W. A. Benjamin, Inc., New York, 1963).

Ritchie, R. H., Private communication (1969).

Ron, A., and N. Tzoar, Phys. Rev. 131, 12 (1963).

Seitz, F., Modern Theory of Solids (McGraw-Hill Book Co., Inc., New York, 1940).

Smith, N. V., and W. E. Spicer, Phys. Rev. Letters 23, 769 (1969).

Stern, F , Solid State Physics (ed. F. Seitz and D. Turnbull) 15, 299 (1963).

Sutherland, J. C., Ph.D. Thesis, Georgia Institute of Technology (1967).

Sutherland, J. C., and E. T. Arakawa, J. Opt. Soc. Am. 58, 1080 (1968).

Sutherland, J. C., R. N. Hamm, and E. T. Arakawa, J. Opt. Soc. Am. 59, 1581 (1969).

Sutton, L., to be published (1969).

Tessman, J. R., A. H. Kahn, and W. Shockley, Phys. Rev. 92, 980 (1953).

Wilson, A. H., Proc. Roy. Soc. (London) 151, 274 (1935).

Wilson, A. H., The Theory of Metals (The Cambridge University Press, Cambridge, 1936; 2nd ed. 1953).

Wood, R. W., Phys. Rev. 44, 353 (1933a).

Wood, R. W., Nature 131, 582 (1933b).

Wood, R. W., and C. Lukens, Phys. Rev. 54, 332 (1938).

Zener, C., Nature 132, 968 (1933).